Journal of Catalysis 283 (2011) 75–88

Contents lists available at ScienceDirect

Journal of Catalysis

journal homepage: www.elsevier.com/locate/jcat

# Kinetic modeling of the total oxidation of propane over Cu- and Ce-based catalysts

V. Balcaen [a], H. Poelman [a,*], D. Poelman [b], G.B. Marin [a]

[a] Laboratory for Chemical Technology, Department of Chemical Engineering, Ghent University, Krijgslaan 281, S5, B-9000 Ghent, Belgium
[b] Department of Solid State Sciences, Ghent University, Krijgslaan 281, S1, B-9000 Ghent, Belgium

ARTICLE INFO

*Article history:*
Received 4 April 2011
Revised 27 June 2011
Accepted 10 July 2011
Available online 20 August 2011

*Keywords:*
Mechanism
Transient kinetic modeling
Propane oxidation
Temporal Analysis of Products
Copper
Ceria

ABSTRACT

The mechanism of the total oxidation of propane over alumina supported CuO, $CeO_2$, and CuO–$CeO_2$ is studied by means of Temporal Analysis of Products in the temperature range 623–873 K. A reaction scheme is proposed for the total oxidation of propane with $O_2$, as well as for the separate reduction and oxidation steps. For the reduction of the catalyst with propane, four elementary steps are considered as kinetically significant: (1) reversible associative propane sorption, (2) irreversible dissociative propane adsorption involving a methylene C–H bond breaking and ultimately forming $CO_2^{*,S}$, (3) desorption of $CO_2^{*,S}$ to $CO_2$, and (4) dissociation of $CO_2^{*,S}$ to $CO^{*,S}$ and $O^{*,S}$, and recombination of $CO^{*,S}$ and $O^{*,S}$ to $CO_2^{*,S}$. For the oxidation of the catalyst with $O_2$, two elementary steps are considered as kinetically significant: (1) reversible dissociative adsorption of $O_2$ on two reduced active sites and (2) diffusion of lattice O atoms from the surface to the bulk and vice versa. An adequate description of the full mechanism, i.e., in the presence of propane and $O_2$, can only be obtained by considering additional steps, which distinguish between lattice oxygen atoms at the surface, $O^{*,S}$, and weakly bound oxygen atoms, $O_{weak}$. Apart from estimating the different kinetic parameters, a new approach to determine the initial concentration of reduced active sites is presented.

CuO–$CeO_2$/$\gamma$-$Al_2O_3$ is a more efficient total oxidation catalyst than the corresponding single metal oxides. The activation energy for the first C–H bond activation in propane over the CuO–$CeO_2$/$\gamma$-$Al_2O_3$ amounts to 62 kJ $mol^{-1}$ and is significantly lower than the activation energies over the single metal oxides, i.e., 95 kJ $mol^{-1}$ for CuO/$\theta$-$Al_2O_3$ and 126 kJ $mol^{-1}$ for $CeO_2$/$\gamma$-$Al_2O_3$. The redox activity of CuO–$CeO_2$/$\gamma$-$Al_2O_3$ is created by the ability to reduce and re-oxidize both CuO and $CeO_2$, which is enhanced by a strong interaction between these phases.



## 1. Introduction

A frequently applied technique to destroy volatile organic compounds (VOCs) is thermal combustion or incineration, requiring temperatures up to 1300 K [1]. Using a catalyst for the oxidation of VOCs allows to significantly reduce the operating temperatures to 600–900 K and to better control the total oxidation. Noble metals or metal oxides are used [2]. The latter are much cheaper, more stable, and resistant to possible toxic by-products [1,2]. High oxygen mobility, easy adsorption, and activation of the VOC to be destroyed, as well as good redox properties that enable the catalyst to undergo reduction and subsequent re-oxidation are desired properties and require the use of mixed metal oxides [3]. Cu-based catalysts are known to be good oxidation catalysts [4,5]. However, the CuO catalyst is very sensitive to the presence of water vapor leading to deactivation [6]. As a pure oxide, ceria is hardly applied because of its textural instability, its high cost, and relatively low activity at lower temperatures [7]. On the other hand, ceria is often present as promoter in the so-called "three-way catalysts" used in automotive industry and plays an important role in CO/NO reactions, oxidative coupling of methane, elimination of $SO_x$ and $NO_x$, and oxidation reactions like CO or hydrocarbon oxidation [8]. According to Trovarelli [8], the most important features of ceria are: lattice ion mobility, easy switching between $Ce^{3+}$ and $Ce^{4+}$, and the high oxidizing power of the $Ce^{4+}$ cation. Demoulin et al. [9] add the ability to generate active O atoms from $CO_2$ to the list of properties which could be of importance in total oxidation reactions.

Combining CuO with $CeO_2$ changes the structure and the redox properties of the catalyst and enhances its activity [10]. CuO–$CeO_2$ catalysts are often used to catalyze various reactions among which CO oxidation [11], VOCs elimination [12], and NO reduction [10] are the most predominant.

In this work, the total oxidation of propane over alumina supported CuO, $CeO_2$, and CuO–$CeO_2$ is studied by means of Temporal Analysis of Products or TAP. A steady-state kinetic study on the same Cu- and Ce-based catalysts has recently been performed by Heynderickx et al. [13]. The TAP technique applied in this work

* Corresponding author. Fax: +32 9 264 4999.
*E-mail address:* Hilde.Poelman@Ugent.be (H. Poelman).

0021-9517/$ - see front matter © 2011 Elsevier Inc. All rights reserved.
doi:10.1016/j.jcat.2011.07.005

**Nomenclature**

| | |
|---|---|
| $A$ | pre-exponential factor (reaction dependent) |
| $cf_p$ | calibration factor of component $p$ (V s mol$^{-1}$) |
| $C_i$ | gas-phase concentration of component $i$ (mol m$_g^{-3}$) |
| $C_{i*}$ | concentration of active sites occupied (mol kg$_c^{-1}$) with species $i$ |
| $C_{O*}$ | concentration of active lattice O atoms (mol kg$_c^{-1}$) |
| $C_{Oweak}$ | concentration of active weakly bound O atoms (mol kg$_c^{-1}$) |
| $C_*$ | concentration of reduced active sites (mol kg$_c^{-1}$) |
| $D^c_{eff,i}$ | effective Knudsen diffusivity in the catalyst bed (m$_g^3$ m$_r^{-1}$ s$^{-1}$) of component $i$ |
| $D^i_{eff,i}$ | effective Knudsen diffusivity in the inert bed (m$_g^3$ m$_r^{-1}$ s$^{-1}$) of component $i$ |
| $E_a$ | activation energy (kJ mol$^{-1}$) |
| $F$ | Fisher's $F$ value (–) |
| $F_i$ | molar flow rate of gas-phase component $i$ (mol s$^{-1}$) |
| $i$ | index of infinite series (–) |
| $j$ | index of infinite series (–) |
| $k$ | index of infinite series (–) |
| $k_n$ | reaction rate coefficient in elementary step $n$ (reaction dependent) |
| $l$ | index of infinite series (–) |
| $L_c$ | length of the catalyst bed ($m_r$) |
| $L_i$ | length of the inert bed at the inlet ($m_r$) |
| $L_o$ | length of the inert bed at the outlet ($m_r$) |
| $m$ | number of gas-phase components (–) |
| $N_{p,i}$ | number of moles $i$ in the pulse (mol) |
| $N$ | total number of observations (–) |
| $n$ | number of experimental conditions (–) |
| $n_p$ | number of pulses per response (–) |
| $n_r$ | number of responses (–) |
| $n_t$ | number of samples per response (–) |
| $p$ | index of infinite series (–) |
| $R$ | universal gas constant (8.314 J mol$^{-1}$ K$^{-1}$) |
| $R_{g,i}$ | specific net production rate of gas-phase (mol kg$_c^{-1}$s$^{-1}$) component $i$ |
| $R_{s,i^*}$ | specific net production rate of surface species $i$ (mol kg$_c^{-1}$s$^{-1}$) |
| $S$ | cross-sectional surface area of the reactor (m$_r^2$) |
| $t$ | time (s) |
| $t_j$ | time between the pulse and the measurement (s) of sample $j$, i.e., sampling time |
| $T$ | temperature (K) |
| $W$ | catalyst weight (kg) |
| $w_i$ | weight factor of response $i$ (–) |
| $Y$ | outlet response (V) |
| $z$ | axial coordinate in the reactor ($m_r$) |

*Greek symbols*

| | |
|---|---|
| $\varepsilon_c$ | void fraction of the catalyst packing (m$_g^3$ m$_r^{-3}$) |
| $\varepsilon_i$ | void fraction of the inert packing (m$_g^3$ m$_r^{-3}$) |
| $\rho$ | binary correlation coefficient (–) |
| $\rho_B$ | density of the catalyst packing (kg$_c$ m$_r^{-3}$) |
| $\sigma_i$ | stoichiometric number of an elementary reaction (–) in global reaction $i$ |
| $\sigma_{ii}$ | stoichiometric number of an elementary reaction (–) or a global reaction in reaction path $ii$ |
| $\tau$ | time scale of reaction or transport (s) |
| $\tau_i$ | time constant of the inlet pulse (s) |
| $\Phi$ | objective function (–) |

*Superscripts*

| | |
|---|---|
| 0 | initial condition |
| b | bulk |
| s | surface |
| t | total |
| ^ | calculated value |

*Subscripts*

| | |
|---|---|
| c | catalyst |
| f | forward |
| max | maximum |
| r | reverse |
| ref | reference |
| trans | transport |
| weak | weakly bound |

allows both qualitative and quantitative investigation at a more fundamental level. Qualitative information obtained on CuO–CeO$_2$/γ-Al$_2$O$_3$ has recently provided further insight in the mechanism of the total oxidation of propane [14]. The purpose of the present work is to describe quantitatively the transient kinetic data with statistically sound kinetic models and physico-chemical meaningful parameters. The kinetically-relevant steps in the proposed mechanisms will be determined as well as the corresponding rate coefficients.

## 2. Experimental

### 2.1. Catalysts

The three catalysts used in this work, CuO–CeO$_2$/γ-Al$_2$O$_3$, CeO$_2$/γ-Al$_2$O$_3$, and CuO/θ-Al$_2$O$_3$ have been extensively characterized in previous publications [13,15,16]. The CuO–CeO$_2$/γ-Al$_2$O$_3$ catalyst was synthesized via impregnation of γ-Al$_2$O$_3$ with Cu(NO$_3$)$_2$ and Ce(NO$_3$)$_3$ precursors, yielding loadings of 9.2 wt.% Cu and 5.2 wt.% Ce, corresponding to 9.31 μmol Cu/m$^2$ and 2.36 μmol Ce/m$^2$, respectively. The supported CeO$_2$ catalyst was obtained by impregnation of γ-Al$_2$O$_3$ with Ce(NO$_3$)$_3$, while the supported CuO was prepared by impregnation of θ-Al$_2$O$_3$ with Cu(NO$_3$)$_2$. Their loadings were 4.8 wt.% Ce and 10.7 wt.% Cu, respectively. All catalyst materials were dried and calcined in air above 873 K.

The total concentration of available lattice oxygen atoms, $C^\circ_{O^*,t}$, is shown in Table 1. It can be assumed to be an upper limit for the total number of exchangeable O atoms. As it was found that the O atoms in the lattice of alumina are not available for reaction [14], only the O atoms related to CuO and/or CeO$_2$ are accounted for without, however, distinguishing between these compounds. The total amount of available lattice oxygen atoms consists of a fraction at the surface, $C^\circ_{O^*,s}$, and in the bulk, $C^\circ_{O^*,b}$. The initial concentration of surface O atoms, $C^\circ_{O^*,s}$, is an important quantity in the kinetic models that will be developed. The values for the different catalysts, see Table 1, are based on XRD and ICP data [14] for determination of the total surface area loaded into the reactor, and on an O surface density for CuO of $7.63 \times 10^{18}$ O atoms m$^{-2}$, and for CeO$_2$ of $8.56 \times 10^{18}$ O atoms m$^{-2}$. The latter values follow from the crystallographic structure of the oxide phase and consider a fully oxidized surface. If the lattice surface is not fully oxidized, a distinction can be made between the initial concentration of reduced active surface sites, $C^\circ_{O^*,s}$, and the initial concentration of active oxygen atoms at the surface.

**Table 1**
Initial concentrations of available lattice O atoms, $C^{\circ}_{O^*,t}$, of lattice O atoms at the surface, $C^{\circ}_{O^*,s}$, and of reduced active surface sites, $C^{\circ}_{*,s}$.

| Catalyst | $C^{\circ}_{O^*,t}$ (mol/kg$_c$) | $C^{\circ}_{O^*,s}$ (mol/kg$_c$) | $C^{\circ}_{*,s}$ (mol/kg$_c$) | |
|---|---|---|---|---|
| | | | 623–873 K [b] | 723–873 K [b] |
| CuO–$CeO_2$/γ-$Al_2O_3$ | 2.20 | $1.32 \times 10^{-1}$ | $(3.25 \pm 0.35) \times 10^{-2}$ | $(3.89 \pm 0.52) \times 10^{-2}$ |
| CuO/θ-$Al_2O_3$ | 1.67 | $4.71 \times 10^{-2}$ | $(1.59 \pm 0.03) \times 10^{-2}$ | $(2.24 \pm 0.06) \times 10^{-2}$ |
| $CeO_2$/γ-$Al_2O_3$ | 0.68 | $7.27 \times 10^{-2}$ | $(4.19 \pm 0.07) \times 10^{-2}$ | $(4.55 \pm 0.09) \times 10^{-2}$ |
| CuO–$CeO_2$/γ-$Al_2O_3$–CuO [a] | 1.46 | $1.40 \times 10^{-2}$ | $4.71 \times 10^{-3}$ | $6.64 \times 10^{-3}$ |
| CuO–$CeO_2$/γ-$Al_2O_3$–$CeO_2$ [a] | 0.74 | $1.18 \times 10^{-1}$ | $6.82 \times 10^{-2}$ | $7.39 \times 10^{-2}$ |

[a] Values reported correspond with the CuO–$CeO_2$/γ-$Al_2O_3$ catalyst, but are only related to CuO and $CeO_2$.
[b] An average of the values estimated during the regression of $O_2$ single-pulse experiments over pre-oxidized catalysts with its 95% confidence interval.

### 2.2. TAP set-up, procedures, and conditions

A detailed description of the TAP technique can be found in [17–19]. In this type of experimental studies, the response of a catalyst to a small perturbation of a certain state variable, e.g., pressure, temperature, or concentration is measured. In TAP experiments, the time-dependent flow rate of the reactants and products is monitored at the reactor outlet by a quadrupole mass spectrometer. The possible detection of gas-phase intermediates of the reaction sequence is one of the advantages of a TAP set-up. Next to this, a TAP experiment indirectly provides information on possible changes in catalyst composition and surface species [19]. Compared to other transient techniques, the TAP technique allows a time resolution in the order of milliseconds, i.e., two orders of magnitude better than conventional transient techniques in heterogeneous catalysis such as temperature-programmed or step-response experiments.

For all tested catalyst samples, a thin-zone reactor configuration is applied [20]. This implies that a sufficiently thin catalyst bed with a typical length of 1/10 of the total reactor length is placed between two beds of inert quartz. The reactor contains 50 mg of catalyst corresponding with 2 to $7 \times 10^{19}$ available O atoms, $O^{*,t}$. The particle diameter of both the catalyst and the quartz pellets is in the range of 250–500 μm. The void fraction of both catalyst and inert beds amounts to 0.53.

In TAP, gas pulses with a width of 100 μs and typically consisting of $10^{14}$–$10^{15}$ molecules per pulse are admitted. This amount of reactants is four orders of magnitude lower than the maximum amount of available O atoms, minimizing the change in the catalyst properties and enabling to study the catalyst at a well-defined state. In the present work, two types of pulse experiments are performed: single- and multi-pulse experiments. In the former, a limited amount of reactant pulses is introduced in order to characterize the catalyst at a predetermined state. By contrast, in a multi-pulse experiment, a large train of pulses is introduced, altering the state of the catalyst.

In the pulse experiments, four different feeds were employed: pure $O_2$, $C_3H_8$ and $CO_2$, next to a mixture of $O_2$ and $C_3H_8$. An experimental program consistently started with an oxidizing sample pretreatment: heating in vacuum to reaction temperature, followed by $O_2$/Ar (50/50) multi-pulse experiment(s) until $O_2$ breakthrough was observed. The state of the pre-oxidized sample was then characterized by an $O_2$/Ar single-pulse experiment at reaction temperature, in which $O_2$ was recorded every 2 pulses. Subsequent single-pulse experiments with $C_3H_8$/Kr (90/10) were always executed 3 min after the $O_2$/Ar single-pulse experiment to investigate the catalysts' state under reducing conditions. Similarly, single-pulse experiments with $CO_2$/Ar (50/50) were performed over a pre-oxidized catalyst, also 3 min after the $O_2$/Ar single-pulse experiment. Single-pulse experiments with a stoichiometric mixture of $O_2$ and $C_3H_8$ were applied to study the total oxidation of propane. In order to investigate the change in catalyst composition in a reducing environment, multi-pulse experiments consisting of 60 $C_3H_8$/Kr pulses were performed, recording propane every six pulses.

The experiments were carried out at temperatures between 623 and 873 K, divided into three ranges: 623–873 K, 723–873 K, and 623–723 K. The $O_2$ single-pulse as well as the $C_3H_8$ multi-pulse experiments were performed over the whole temperature range. For the $C_3H_8$ single-pulse experiments, the whole range, 623–873 K, was considered if $CO_2$ desorption was neglected, and 723–873 K, if $CO_2$ responses with their complete tail were recorded. The latter appeared impossible at the lower temperatures, because only weak $CO_2$ responses that could hardly be distinguished from the noise level were obtained. The $CO_2$ single-pulse experiments were only executed between 723 and 873 K for similar reasons. The $O_2$/propane single-pulse experiments were executed between 623 and 723 K, in order to investigate the influence of weakly bound oxygen atoms upon catalytic activity. As a consequence, $CO_2$ responses were not available.

The different gases at the outlet were monitored, focusing on the following masses: 18 AMU for water, 28 for CO, 29 for $C_3H_8$, 32 for $O_2$, 40 for Ar, 41 for $C_3H_6$, 44 for $CO_2$, and 84 AMU for Kr. Inert gases were used as internal standard. From mass 41 and 44, the contribution of propane is subtracted, i.e., 15–18%, respectively, 27–30% of the peak at 29 AMU depending on the calibration in order to obtain the pure response signals of $C_3H_6$ and $CO_2$, respectively. From mass 28, 63% of the peak at 29 AMU and 22% of the peak at 44 AMU related to pure $CO_2$ is subtracted to obtain the pure response signal of CO at 28 AMU. These corrections are only necessary if the response signals measured in voltage are transformed to outlet flow rates of the different gases.

## 3. Kinetic parameter estimation

### 3.1. Modeling of pulse responses: regression analysis

The reactor model applied to model the TAP pulse responses is represented in Fig. 1. The model uses an identical set of partial differential equations in each zone of the reactor as applied in Balcaen et al. [21]:

$$\varepsilon_i \frac{\partial C_A}{\partial t} = D^i_{eff,A} \frac{\partial^2 C_A}{\partial z^2} \quad 0 < z < L_i \tag{1}$$

$$\varepsilon_c \frac{\partial C_A}{\partial t} = D^c_{eff,A} \frac{\partial^2 C_A}{\partial z^2} + \rho_B R_{g,A} \quad L_i < z < L_i + L_c \tag{2}$$

$$\varepsilon_i \frac{\partial C_A}{\partial t} = D^i_{eff,A} \frac{\partial^2 C_A}{\partial z^2} \quad L_i + L_c < z < L_i + L_c + L_o \tag{3}$$

$$\frac{\partial C_{A^*}}{\partial t} = R_{s,A^*} \quad L_i < z < L_i + L_c \tag{4}$$

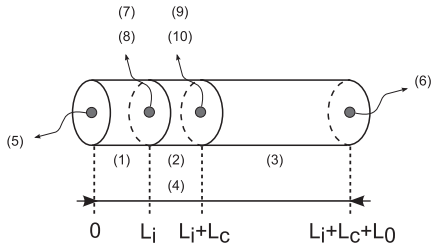


**Fig. 1.** TAP reactor model applied for modeling the pulse responses with indication of the different zones. The numbers in brackets refer to the partial differential equations, boundary conditions, and transmission conditions between beds as mentioned in Section 3.1.

with following boundary conditions at the inlet, Eq. (5) and the outlet, Eq. (6) of the reactor:

$$-SD^{i}_{eff,A}\left(\frac{\partial C_A}{\partial z}\right)=\frac{N_{p,A}}{\tau_i^2}t\exp\left(-\frac{t}{\tau_i}\right)\quad t\geqslant 0, z=0 \tag{5}$$

$$C_A=0\quad t\geqslant 0, z=L_i+L_c+L_o \tag{6}$$

The transmission conditions between the beds are given by Eqs. (7)–(10),

$$(C_A)_{z=L_{i-}}=(C_A)_{z=L_{i+}} \tag{7}$$

$$\left(D^{i}_{eff,A}\frac{\partial C_A}{\partial z}\right)_{z=L_{i-}}=\left(D^{c}_{eff,A}\frac{\partial C_A}{\partial z}\right)_{z=L_{i+}} \tag{8}$$

$$(C_A)_{z=(L_i+L_c)-}=(C_A)_{z=(L_i+L_c)+} \tag{9}$$

$$\left(D^{c}_{eff,A}\frac{\partial C_A}{\partial z}\right)_{z=(L_i+L_c)-}=\left(D^{i}_{eff,A}\frac{\partial C_A}{\partial z}\right)_{z=(L_i+L_c)+} \tag{10}$$

and the initial conditions by Eq. (11):

$$C_A=0\quad C_{A^*}=C^0_{A^*}\quad t=0,\ 0\leqslant z\leqslant L_i+L_c+L_o \tag{11}$$

The reactor model equations are integrated in the time domain by applying the method of lines. In the inert zones of the reactor, the concentration of every gas-phase component is solely influenced by Knudsen diffusion. In the catalyst zone of the reactor, apart from diffusion, also other processes need to be accounted for, i.e., adsorption, desorption, and reaction. Therefore, in the partial differential equations corresponding with the catalyst zone, the specific net production rates of the gas-phase and the surface components, $R_{g,A}$ and $R_{s,A^*}$, are inserted. The derivation of these net production rates depends on the proposed reaction network with its kinetically significant steps, see Section 4. A step is called kinetically significant if the rate coefficient influences the calculated responses.

The parameters of the several kinetically significant steps are estimated using the Levenberg–Marquardt [22] method for the minimization of the objective function, $\Phi$, presented by Eq. (12) according to [23]:

$$\Phi=\sum_{i=1}^{n_r}\sum_{j=1}^{N(i)}\left(Y_{i,j}-\widehat{Y}_{i,j}\right)^2 \tag{12}$$

In this work, a non-weighted, non-linear least-squares regression is performed. The total number of observations per response $i$, $N(i)$, can be specified in more detail, giving rise to Eq. (13):

$$\Phi=\sum_{i=1}^{n_r}\sum_{k=1}^{n}\sum_{l=1}^{n_p}\sum_{j=1}^{n_t(i)}\left(Y_{i,k,l}(t_j)-\widehat{Y}_{i,k,l}(t_j)\right)^2 \tag{13}$$

where

$$N(i)=n\,n_p\,n_t(i) \tag{14}$$

$$Y_{i,k,l}(t_j)=\sum_{p=1}^{m}cf_pF_{p,k,l}(t_j)=\sum_{p=1}^{m}cf_p\left(-D_{eff,p,k,l}S\frac{\partial C_{p,k,l}(t_j)}{\partial z}\right) \tag{15}$$

is the observed response and

$$\widehat{Y}_{i,k,l}(t_j)=\sum_{p=1}^{m}cf_p\widehat{F}_{p,k,l}(t_j)=\sum_{p=1}^{m}cf_p\left(-D_{eff,p,k,l}S\frac{\partial\widehat{C}_{p,k,l}(t_j)}{\partial z}\right) \tag{16}$$

is the calculated response corresponding to mass $i$, followed by the mass spectrometer.

If the number of responses, $n_r$, equals 1, a single-response regression analysis is performed. If more than one response is considered, the regression is called multi-response. The responses are measured by sampling at equidistant times, $t_j$, per set of experimental conditions, $k$, and per pulse number, l. The regression analysis is not limited to single-pulse experiments, but can also treat multi-pulse data. In the former, the number of pulses per response, $n_p$, equals 1, while in the latter, $n_p$ is higher than 1. Hence, apart from state-defining experiments, also state-altering experiments can be modeled in order to describe the evolution of a catalyst surface.

It must be stressed that in contrast to the non-linear, multi-response multiple regression analysis performed in [21], the least-squares criterion in this work is applied to the responses, $Y$, expressed in voltage, instead of to the outlet flow rates, $F$.

If non-isothermal regression is performed, a reparametrization is applied to minimize the correlation between the pre-exponential factor and the activation energy, according to Eq. (17):

$$k_n=k_{n,T_{ref}}\exp\left(-\frac{E_a}{R}\left(\frac{1}{T}-\frac{1}{T_{ref}}\right)\right) \tag{17}$$

where $T_{ref}$ is the average of the temperatures considered in the regression.

### 3.2. Evaluation of the regression

The performed regressions are evaluated by executing some typical statistical tests [23,24] and further by interpreting the obtained kinetic parameter values from physico-chemical point of view.

In the statistical evaluation, the significance of the regression is evaluated using the $F$ test for the global significance and the $t$ test for the significance of the individual parameter estimates. The correlation between different parameters in a given model must be sufficiently low. If several reaction networks are a priori possible, leading to a number of possible kinetic models, discrimination among the rival models is based on the Bayesian information criterion (BIC) [25]. This criterion not only takes into account the difference in the residual sum of squares between competing models, but also accounts for a possible difference in number of parameters. The model with the lowest value of BIC is selected. Instead of reporting the absolute BIC values, the differences $\Delta$BIC between the absolute value of every other model and the model with the lowest BIC value will be listed.

## 4. Reaction networks and rate equations

Fig. 2 presents a set of reaction schemes for the oxidation of the catalysts with $O_2$, see Fig. 2a and Table 2, for the reduction with propane, see Fig. 2b and Table 3, for the oxidation with $CO_2$, and for the total oxidation with a propane/$O_2$ mixture, see Fig. 2c, showing possible steps that can occur under these different conditions. Only kinetically-relevant steps in the reaction network are displayed, while intermediate, kinetically non-significant steps are replaced by progressing dots.

During single-pulse experiments, no gas-phase CO has been detected, so the elementary reaction $CO^{*,s}\rightarrow CO+*,s$ is not accounted for. Likewise, negligible amounts of detected gas-phase propylene have led to the omission of any elementary reaction resulting in

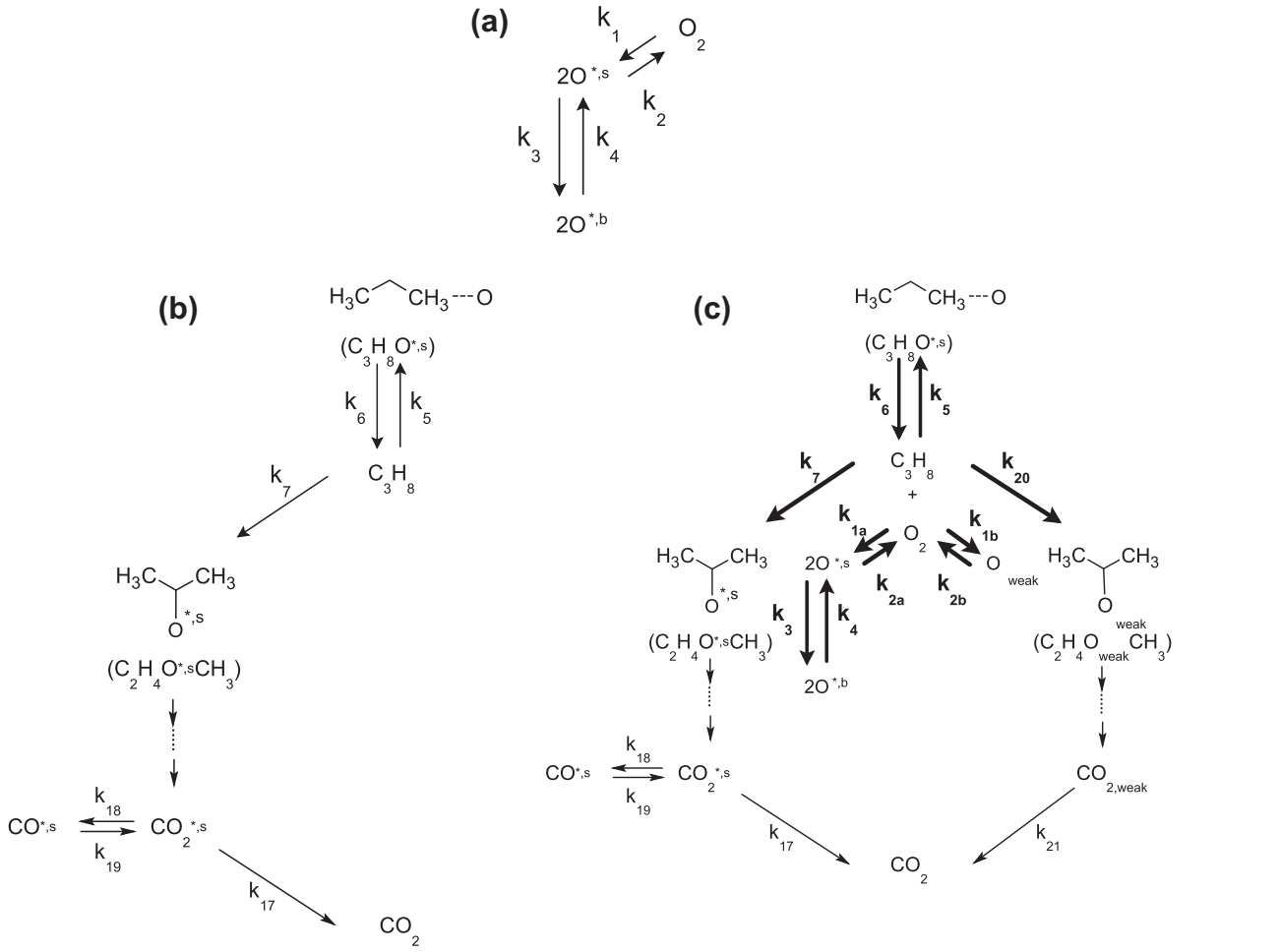


**Fig. 2.** Set of reaction schemes: (a) reaction network for the oxidation of the catalysts with $O_2$; (b) reaction scheme for the reduction of the catalysts with propane; the intermediate, kinetically non-significant steps are not represented but rather indicated by progressing dots in between the arrows; (c) proposed reaction network for the total oxidation of propane over CuO–$CeO_2$/γ-$Al_2O_3$ with indication of the kinetically significant steps corresponding to reduction, steps (5)–(7) and (17)–(21), next to re-oxidation, steps (1a), (1b), (2a), (2b), (3), and (4), now involving both surface lattice oxygen, $O^{*,s}$, as well as weakly bound oxygen atoms, $O_{weak}$. The latter O species were required to obtain an adequate description of the responses. The steps related to the activation of propane by $O^{*,s}$ are identical to the steps presented in Table 3. Only estimation of the rate coefficients of the steps shown in bold was possible during the non-isothermal multi-response regression of propane/$O_2$ single-pulse experiments. The intermediate, kinetically non-significant steps are not represented but rather indicated by progressing dots in between the arrows.

the production of propene. Readsorption of propene and subsequent formation of $CO_2$ are not considered either as during the kinetic modeling the propane and $CO_2$ responses could be adequately described without such elementary steps. As water cannot be detected as a response to a pulse on the time scale of a TAP single-pulse experiment, the elementary reaction $2HO^{*,S} \rightarrow H_2O + O^{*,S} + *,s$ is also omitted from the reaction schemes. This will not influence the regression of single-pulse experiments since the HO coverage is not significantly altered, by limiting the number of admitted reactant molecules relative to the number of active sites in the reactor. On the other hand, in the multi-pulse experiments, the HO coverage is expected to change during the

**Table 2**
Elementary reactions (1)–(4) during the re-oxidation of CuO–$CeO_2$/γ-$Al_2O_3$, CuO/θ-$Al_2O_3$, and $CeO_2$/γ-$Al_2O_3$ with $O_2$. The corresponding scheme is represented in Fig. 2a. All presented steps are kinetically significant.

| | |
|---|---|
| $O_2 + 2^*,s \rightarrow 2O^{*,s}$ | (1) |
| $2O^{*,s} \rightarrow O_2 + 2^*,s$ | (2) |
| $O^{*,s} \rightarrow O^{*,b}$ | (3) |
| $O^{*,b} \rightarrow O^{*,s}$ | (4) |

**Table 3**
Elementary reactions (5)–(19) considered during the reduction of CuO–$CeO_2$/γ-$Al_2O_3$, CuO/θ-$Al_2O_3$, and $CeO_2$/γ-$Al_2O_3$ with propane with corresponding global reactions (α and β) and reaction paths (αα and ββ). The corresponding scheme is represented in Fig. 2b. Kinetically significant steps are shown in bold.

| | $\sigma_\alpha$ | $\sigma_\beta$ | |
|---|---|---|---|
| **$C_3H_8 + O^{*,s} \rightarrow C_3H_8O^{*,s}$** | **1** | 0 | (5) |
| **$C_3H_8O^{*,s} \rightarrow C_3H_8 + O^{*,s}$** | **1** | 0 | (6) |
| **$C_3H_8 + 2O^{*,s} \rightarrow C_2H_4O^{*,s}CH_3 + HO^{*,s}$** | 0 | **1** | (7) |
| $C_2H_4O^{*,s}CH_3 + O^{*,s} \rightarrow C_2H_4O^{*,s}CH_2 + HO^{*,s}$ | 0 | 1 | (8) |
| $C_2H_4O^{*,s}CH_2 + O^{*,s} \rightarrow C_2H_4O^{*,s} + CH_2O^{*,s}$ | 0 | 1 | (9) |
| $C_2H_4O^{*,s} + O^{*,s} \rightarrow C_2H_4(O^{*,s})_2$ | 0 | 1 | (10) |
| $C_2H_4(O^{*,s})_2 + 2O^{*,s} \rightarrow C_2H_3(O^{*,s})_3 + HO^{*,s}$ | 0 | 1 | (11) |
| $C_2H_3(O^{*,s})_3 + 2O^{*,s} \rightarrow C_2H_2(O^{*,s})_4 + HO^{*,s}$ | 0 | 1 | (12) |
| $C_2H_2(O^{*,s})_4 \rightarrow 2CH(O^{*,s})_2$ | 0 | 1 | (13) |
| $CH_2O^{*,s} + O^{*,s} \rightarrow CH_2(O^{*,s})_2$ | 0 | 1 | (14) |
| $CH_2(O^{*,s})_2 + O^{*,s} \rightarrow CH(O^{*,s})_2 + HO^{*,s}$ | 0 | 1 | (15) |
| $CH(O^{*,s})_2 + O^{*,s} \rightarrow CO_2^{*,s} + HO^{*,s} + ^*,s$ | 0 | 3 | (16) |
| | $\sigma_{\alpha\alpha}$ | $\sigma_{\beta\beta}$ | |
| **$C_3H_8O^{*,s} \rightleftarrows C_3H_8O^{*,s}$** | **1** | 0 | (α) |
| **$C_3H_8 + 14O^{*,s} \rightarrow 3CO_2^{*,s} + 8HO^{*,s} + 3^*,s$** | 0 | **1** | (β) |
| **$CO_2^{*,s} \rightarrow CO_2 + ^*,s$** | 0 | **3** | (17) |
| **$CO_2^{*,s} + ^*,s \rightarrow CO^{*,s} + O^{*,s}$** | 0 | **3** | (18) |
| **$CO^{*,s} + O^{*,s} \rightarrow CO_2^{*,s} + ^*,s$** | 0 | **3** | (19) |
| $C_3H_8 + O^{*,s} \rightleftarrows C_3H_8O^{*,s}$ | | | (αα) |
| $C_3H_8 + 14O^{*,s} \rightarrow 3CO_2 + 8HO^{*,s} + 6^*,s$ | | | (ββ) |

course of the experiments. However, if it is assumed that water mostly adsorbs on the alumina support, the presence of hydroxyl groups will not influence the catalytic activity. The strong adsorption of water on alumina is well documented [5].

### 4.1. Oxygen feed

A reaction scheme for the oxidation of the catalyst with $O_2$ is proposed in Fig. 2a and Table 2. In this simplified scheme, no distinction is made between surface lattice oxygen, $O^{*,s}$, and $O_{weak}$, referring to both weakly bound oxygen atoms in the surface lattice and adsorbed oxygen from the gas phase. These $O_{weak}$ species are only important when propane and oxygen are introduced simultaneously.

In the proposed scheme, $O_2$ reacts with reduced active surface sites, $^*$,s, to form surface lattice oxygen, $O^{*,s}$, according to step (1). This surface lattice oxygen can either desorb from the catalyst, step (2), or diffuse to the subsurface or bulk of the catalyst and vice versa, steps (3) and (4). In order to model this diffusion, similar model equations as proposed by Dewaele et al. [26] are applied, rather than Fick's second law, see Mills et al. [27] and Nibbelke et al. [28]. The transport is described with two elementary steps and corresponding rate coefficients.

The above reaction scheme leads to the following expressions for the specific net production rates:

$$R_{g,O_2} = -k_1 C_{O_2} C_{*,s}^2 + k_2 C_{O^{*,s}}^2 \quad (18)$$

$$R_{s,O^{*,s}} = 2k_1 C_{O_2} C_{*,s}^2 - 2k_2 C_{O^{*,s}}^2 - k_3 C_{O^{*,s}} + k_4 C_{O^{*,b}} \quad (19)$$

$$R_{s,^{*,s}} = -2k_1 C_{O_2} C_{*,s}^2 + 2k_2 C_{O^{*,s}}^2 \quad (20)$$

$$R_{s,O^{*,b}} = k_3 C_{O^{*,s}} - k_4 C_{O^{*,b}} \quad (21)$$

### 4.2. Propane feed

#### 4.2.1. Single-pulse experiments

A reaction scheme for the reduction of the catalyst with propane is proposed in Fig. 2b and Table 3. The elementary reactions denoted by numbers (5)–(19) are combined to obtain the global reactions designated by the Greek symbols $\alpha$ and $\beta$, taking into account the stoichiometric numbers, $\sigma_i$. These global reactions can be combined with elementary reactions according to the stoichiometric numbers, $\sigma_{ii}$, to obtain the reaction paths $\alpha\alpha$ and $\beta\beta$. Multiresponse regression of the experimental propane and $CO_2$ responses has been performed with different, a priori possible, kinetically significant steps leading to several expressions for the net production rates, $R_{g,A}$ and $R_{s,A^*}$. Selection between the obtained kinetic models is based on the Bayesian information criterion and the correspondence between the experimental data and the calculated responses. Considering the steps shown in bold in the reaction scheme of Table 3 as kinetically significant provided the best description of the experimental propane and $CO_2$ responses.

Reaction path ($\alpha\alpha$) consists of two kinetically significant elementary steps. In the first step (5), propane adsorbs on one active surface oxygen atom, $O^{*,s}$, without bond breaking, from which it can desorb, elementary step (6). This reaction path only involves adsorption/desorption of propane without the production of $CO_2$, and thus will not be of great importance when the activity of a catalyst toward the total oxidation of propane is evaluated. However, the steps appeared necessary to adequately describe the experimental propane responses.

Reaction path ($\beta\beta$) describes the actual total oxidation of propane through global reaction ($\beta$) combined with the elementary reactions (17)–(19). In the global reaction ($\beta$), the methylene C–H bond breaking, elementary step (7) is assumed to be kinetically relevant. This is in agreement with the results published by Finocchio et al. [29] who stated that propane activation on transition metal oxides occurs via initial cleavage of the methylene C–H bond as this bond is weaker than the methyl C–H bond. In this step, propane interacts with two surface oxygen atoms, $O^{*,s}$, leading to a second-order dependency on the concentration of $O^{*,s}$. This interaction will be much stronger compared to that in step (5), as it leads to further reaction of propane to $CO_2$. Moreover, the methylene C–H bond breaking, step (7), is irreversible as the reverse step could not be significantly estimated. After the first C–H bond activation in propane, the resulting intermediate instantaneously transforms to $CO_2^{*,s}$, which desorbs in step (17). Alternatively, $CO_2^{*,s}$ can dissociate to $CO^{*,s}$ and $O^{*,s}$ in step (18), which is reversible through step (19).

The corresponding specific net production rates of the gas-phase, $R_{g,A}$, and the surface components, $R_{s,A*}$, are given by Eqs. (22)–(28):

$$R_{g,C_3H_8} = -k_5 C_{C_3H_8} C_{O^{*,s}} + k_6 C_{C_3H_8O^{*,s}} - k_7 C_{C_3H_8} C_{O^{*,s}}^2 \quad (22)$$

$$R_{g,CO_2} = k_{17} C_{CO_2^{*,s}} \quad (23)$$

$$R_{s,C_3H_8O^{*,s}} = k_5 C_{C_3H_8} C_{O^{*,s}} - k_6 C_{C_3H_8O^{*,s}} \quad (24)$$

$$R_{s,O^{*,s}} = -k_5 C_{C_3H_8} C_{O^{*,s}} + k_6 C_{C_3H_8O^{*,s}} - 14k_7 C_{C_3H_8} C_{O^{*,s}}^2 + k_{18} C_{CO_2^{*,s}} C_{*,s} - k_{19} C_{CO^{*,s}} C_{O^{*,s}} \quad (25)$$

$$R_{s,CO_2^{*,s}} = 3k_7 C_{C_3H_8} C_{O^{*,s}}^2 - k_{17} C_{CO_2^{*,s}} - k_{18} C_{CO_2^{*,s}} C_{*,s} + k_{19} C_{CO^{*,s}} C_{O^{*,s}} \quad (26)$$

$$R_{s,CO^{*,s}} = k_{18} C_{CO_2^{*,s}} C_{*,s} - k_{19} C_{CO^{*,s}} C_{O^{*,s}} \quad (27)$$

$$R_{s,^{*,s}} = 3k_7 C_{C_3H_8} C_{O^{*,s}}^2 + k_{17} C_{CO_2^{*,s}} - k_{18} C_{CO_2^{*,s}} C_{*,s} + k_{19} C_{CO^{*,s}} C_{O^{*,s}} \quad (28)$$

When $CO_2$ desorption is neglected, the kinetic model consists of Eqs. (22), (24), and (25), omitting the two last terms in the right-hand side of Eq. (25).

#### 4.2.2. Multi-pulse experiments

Compared to the reaction scheme for the propane single-pulse experiments, two extra steps are added to the scheme when multi-pulse experiments are considered. These two steps are analogous to the steps in the reaction scheme for $O_2$ single-pulse experiments, steps (3) and (4) in Table 2. This leads to following specific net production rates:

$$R_{g,C_3H_8} = -k_5 C_{C_3H_8} C_{O^{*,s}} + k_6 C_{C_3H_8O^{*,s}} - k_7 C_{C_3H_8} C_{O^{*,s}}^2 \quad (29)$$

$$R_{s,C_3H_8O^{*,s}} = k_5 C_{C_3H_8} C_{O^{*,s}} - k_6 C_{C_3H_8O^{*,s}} \quad (30)$$

$$R_{s,O^{*,s}} = -k_5 C_{C_3H_8} C_{O^{*,s}} + k_6 C_{C_3H_8O^{*,s}} - 14k_7 C_{C_3H_8} C_{O^{*,s}}^2 - k_3 C_{O^{*,s}} + k_4 C_{O^{*,b}} \quad (31)$$

$$R_{s,O^{*,b}} = k_3 C_{O^{*,s}} - k_4 C_{O^{*,b}} \quad (32)$$

### 4.3. Carbon dioxide feed

Next to $O_2$, $CO_2$ also acts as an oxidizing agent over the CuO–$CeO_2$/$\gamma$-$Al_2O_3$ catalyst [14]. The responses for $CO_2$ feed over pre-oxidized catalyst are modeled starting from the steps in the network described in Section 4.2.1, i.e., elementary reactions (17)–(19) from Table 3, and adding the adsorption of $CO_2$ : $CO_2 + {}^*, s \rightarrow CO_2^{*,s}$.

The following net production rates are inserted in the reactor model to describe the $CO_2$ responses:

$$R_{g,CO_2} = -k_{f,17} C_{CO_2} C_{*,s} + k_{r,17} C_{CO_2^{*,s}} \quad (33)$$

$$R_{s,^{*,s}} = -k_{f,17} C_{CO_2} C_{*,s} + k_{r,17} C_{CO_2^{*,s}} - k_{18} C_{CO_2^{*,s}} C_{*,s} + k_{19} C_{CO^{*,s}} C_{O^{*,s}} \quad (34)$$

$$R_{s,O^{*,s}} = k_{18}C_{CO_2^{*,s}}C_{*,s} - k_{19}C_{CO^{*,s}}C_{O^{*,s}} \quad (35)$$

$$R_{s,CO_2^{*,s}} = k_{f,17}C_{CO_2}C_{*,s} - k_{r,17}C_{CO_2^{*,s}} - k_{18}C_{CO_2^{*,s}}C_{*,s} + k_{19}C_{CO^{*,s}}C_{O^{*,s}} \quad (36)$$

$$R_{s,CO^{*,s}} = k_{18}C_{CO_2^{*,s}}C_{*,s} - k_{19}C_{CO^{*,s}}C_{O^{*,s}} \quad (37)$$

In these equations, an identical numbering for the rate coefficients of the kinetically significant steps is applied as presented in Table 3, except for the additional adsorption step of $CO_2$. The rate coefficient of this forward step is denoted by $k_{f,17}$, while the reverse step is denoted by $k_{r,17}$.

### 4.4. Oxygen/propane mixture

In a stoichiometric $O_2$/propane atmosphere, catalyst reduction by propane and oxidation by $O_2$ will simultaneously occur via the steps discussed in the previous sections. However, considering only the latter, no adequate description of the mechanism could be obtained. Hence, additional steps had to be added, more specifically to the networks described in Sections 4.1 and 4.2.1: $O_2 \leftrightarrows O_{weak}$ and $C_3H_8 + 2O_{weak} \rightarrow C_2H_4O_{weak}CH_3 + HO_{weak}$. In addition to the lattice oxygen atoms at the surface of the catalyst, $O^{*,s}$, weakly bound oxygen atoms, $O_{weak}$, need to be considered in order to obtain an adequate description of the experimental propane and $O_2$ responses. These $O_{weak}$ atoms are activated oxygen atoms to be found near and related to surface lattice oxygen, $O^{*,s}$, which exist specifically on freshly oxidized material. Pantazidis et al. [30] considered similar oxygen atoms involved in the activation of propane over a V–Mg–O catalyst. These authors suggested that lattice oxygen atoms are involved in the selective propane-to-propene route, while the activated oxygen atoms, denoted as superoxidized forms of the oxidized lattice sites, are responsible for the non-selective route of propane to $CO_x$. However, as only negligible amounts of propene were detected over all catalysts investigated in the present study, it must be concluded that both types of oxygen atoms are involved in the total oxidation of propane in contrast to [30]. The $O_{weak}$ atoms will only be of importance on a pre-oxidized sample, whereas on a partly reduced catalyst surface, the strong incorporation of oxygen atoms into the lattice will be so fast that the number of weakly bound $O_{weak}$ atoms can be neglected [31]. Liu and Flytzani-Stephanopoulos [11] associate the formation of such atoms to the presence of $Ce^{4+}$, but their generation at the CuO–$CeO_2$ interface has also been reported [32,33]. Because of the uncertainty of where the $O_{weak}$ atoms are formed, the number of sites on which these atoms can be created will not be explicitly considered in the kinetic model. Instead, it will be assumed that this number remains constant during a single-pulse experiment and, hence, the product of this number and the rate coefficient will be estimated. This assumption is justified as the number of reactant molecules introduced during one pulse is negligible compared to the number of active sites in the reactor.

The kinetically significant steps for propane total oxidation are summarized in Fig. 2c, in which both reduction and oxidation schemes are combined, presenting a complete reaction network. The extra step related to the activation of propane by $O_{weak}$ is denoted by number (20), while the other steps are assigned identical numbers as in Tables 2 and 3. Because of the distinction between $O^{*,s}$ and $O_{weak}$, in steps (1) and (2) of Table 2, a distinction is now made between step (1a)–(1b) and (2a)–(2b). For the adsorbed $CO_2$ formed by interaction of propane with $O_{weak}$, it is assumed that these $CO_{2,weak}$ species will rather desorb from the surface than dissociate, see step (21). For the weakly bound O atoms, $O_{weak}$, transformation to bulk oxygen atoms is not considered as these atoms will either directly react with propane to form $CO_2$ or desorb, rather than diffuse into the bulk of the catalyst.

Because between 623 and 723 K, only propane and oxygen responses are available, an estimation of the rate coefficients is only possible for the steps presented in bold in Fig. 2c. Moreover, some of these elementary reactions are identical to steps from the reaction network of reduction, i.e., steps (5)–(7) from Table 3, and the corresponding rate coefficients will not be estimated. The parameters of steps (3) and (4) will not be estimated either for similar reasons. Instead, their values will be fixed to the values obtained under reduction and oxidation conditions, resulting in the following parameters to be estimated by regression of the responses to oxygen/propane pulses: $k_{20}$ for the activation of propane by $O_{weak}$, $k_{1a}$ and $k_{1b}$ for the activation of $O_2$ to $O^{*,s}$ and $O_{weak}$ atoms and $k_{2a}$ and $k_{2b}$ for the possible desorption of these atoms, respectively. It should be stressed that the parameter $k_{1b}$ is a product of a rate coefficient and a concentration of the active sites on which the weakly bound oxygen atoms are formed. The specified parameters will be estimated by multi-response regression, applying the following expressions for the net production rates:

$$R_{g,C_3H_8} = -k_5C_{C_3H_8}C_{O^{*,s}} + k_6C_{C_3H_8O^{*,s}} - k_7C_{C_3H_8}C^2_{O^{*,s}} - k_{20}C_{C_3H_8}C^2_{O_{weak}} \quad (38)$$

$$R_{g,O_2} = -k_{1a}C_{O_2}C^2_{*,s} + k_{2a}C^2_{O^{*,s}} - k_{1b}C_{O_2} + k_{2b}C_{O_{weak}} \quad (39)$$

$$R_{s,O^{*,s}} = -k_5C_{C_3H_8}C_{O^{*,s}} + k_6C_{C_3H_8O^{*,s}} - 14k_7C_{C_3H_8}C^2_{O^{*,s}} + 2k_{1a}C_{O_2}C^2_{*,s} - 2k_{2a}C^2_{O^{*,s}} - k_3C_{O^{*,s}} + k_4C_{O^{*,b}} \quad (40)$$

$$R_{s,O_{weak}} = -14k_{20}C_{C_3H_8}C^2_{O_{weak}} + k_{1b}C_{O_2} - k_{2b}C_{O_{weak}} \quad (41)$$

$$R_{s,C_3H_8O^{*,s}} = k_5C_{C_3H_8}C_{O^{*,s}} - k_6C_{C_3H_8O^{*,s}} \quad (42)$$

$$R_{s,*,s} = 3k_7C_{C_3H_8}C^2_{O^{*,s}} - 2k_{1a}C_{O_2}C^2_{*,s} + 2k_{2a}C^2_{O^{*,s}} \quad (43)$$

$$R_{s,O^{*,b}} = k_3C_{O^{*,s}} - k_4C_{O^{*,b}} \quad (44)$$

## 5. CuO–$CeO_2$/γ-$Al_2O_3$

### 5.1. Oxygen feed

#### 5.1.1. Estimation of the initial concentration of reduced active sites: isothermal regression

Despite the oxidizing pretreatment, a pre-oxidized catalyst is not completely oxidized due to desorption of lattice oxygen at the investigated conditions. The latter reduction is induced by the vacuum environment of the TAP analysis chamber, causing the catalyst to release its oxygen [14]. This implies that a $C_3H_8$ or a $CO_2$ experiment, performed 3 min after the pre-oxidation, is not executed over a completely oxidized catalyst surface, but over a surface partly consisting of reduced active sites. Hence, it is

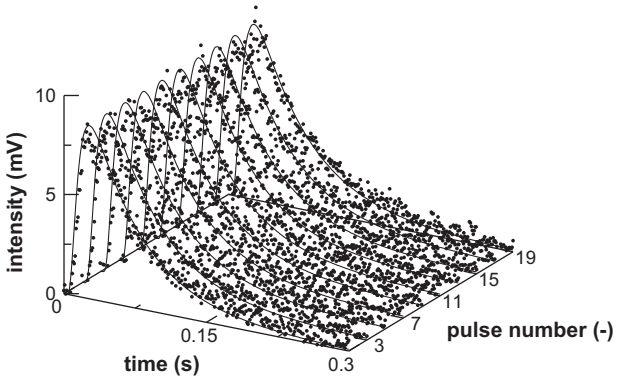


**Fig. 3.** $O_2$ responses at 623 K over pre-oxidized CuO–$CeO_2$/γ-$Al_2O_3$ corresponding to an $O_2$/Ar single-pulse experiment consisting of 20 pulses with the $O_2$ response monitored every two pulses. (●) Experimental $O_2$ responses; (–) responses calculated with parameter estimates reported in Tables 1 and 4, obtained by isothermal and non-isothermal single-response regression, and Eqs. (1)–(4) with the corresponding net production rates, Eqs. (18)–(21).

necessary to determine the initial concentration of reduced active sites, $C^{\circ}_{*,s}$. To this end, a state-defining $O_2$/Ar single-pulse experiment consisting of ten $O_2$ pulses, performed after the pre-oxidation, was modeled using the reaction network presented in Table 2. Apart from the kinetic rate coefficients, $C^{\circ}_{*,s}$ was estimated for every reaction temperature during the isothermal regression. In the $O_2$/Ar single-pulse experiment, ten identical oxygen responses were obtained, indicating that the concentration of O atoms and reduced active sites in the catalyst bed was not affected during the course of the single-pulse experiment. Indeed, a satisfying correspondence between the experimental and calculated responses, presented in Fig. 3 for the CuO–$CeO_2$/γ-$Al_2O_3$ at 623 K, was obtained only for values of the estimated initial concentration of reduced active sites, $C^{\circ}_{*,s}$, that were sufficiently high compared to the pulsed number of $O_2$ molecules. For all temperatures between 623 and 873 K and for all catalysts, the initial concentration of reduced surface sites could be significantly estimated as an additional parameter next to the kinetic parameters with satisfying 95% confidence intervals. The kinetic parameters corresponding to the isothermal regression are not explicitly listed as the correspondence with the non-isothermal estimates was very good.

As expected, isothermal estimation resulted in values for $C^{\circ}_{*,s}$ which increased with temperature. However, because the increase was fairly moderate, two average values were applied as initial conditions for the reduced catalyst sites during the non-isothermal modeling: a first average for the 623–873 K temperature range and a second for the 723–873 K range. In Table 1, these average values are reported and the small difference between the two values confirms the limited temperature dependency of $C^{\circ}_{*,s}$. It appeared unnecessary to apply a third average value for the temperature range 623–723 K, because of negligible difference compared to the value obtained between 623 and 873 K. Depending on the considered temperature range, the ratio of the initially reduced active sites to the total number of surface lattice oxygen atoms varies from 25% to 29%.

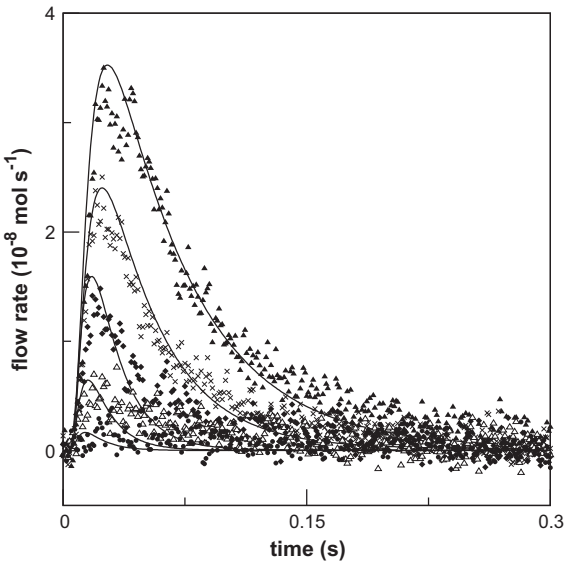


**Fig. 4.** $O_2$ reactor exit flow rates corresponding to $O_2$ single-pulse experiments over pre-oxidized CuO–$CeO_2$/γ-$Al_2O_3$ at (▲) 623, (×) 673, (♦) 773, (Δ) 823, and (●) 873 K. Experimental $O_2$ responses are presented by symbols; (–) $O_2$ responses calculated with parameter estimates reported in Tables 1 and 4, obtained by isothermal and non-isothermal single-response regression, and Eqs. (1)–(4) with the corresponding net production rates, Eqs. (18)–(21).

### 5.1.2. Non-isothermal regression

Fig. 4 shows the good correspondence between the experimental and calculated transient $O_2$ responses over pre-oxidized CuO–$CeO_2$/γ-$Al_2O_3$ after non-isothermal regression analysis of $O_2$ single-pulse experiments, and Table 4 lists the corresponding parameter estimates. It must be stressed that a very broad temperature interval ranging from 623 up to 873 K can be well described using a single mechanism and a single set of kinetic parameter values.

The activation of $O_2$ by adsorption on two reduced catalytic sites is an activated process with a value of $E_{a,1}$ of 66.2 kJ mol$^{-1}$. The rate coefficient of the subsequent desorption is quite low in comparison to the value of adsorption. The activation energy of the $O_2$ desorption cannot be estimated significantly different from zero at 95% probability level. This is in line with the moderate temperature dependency obtained for $C^{\circ}_{*,s}$, see Table 1.

It is found that $k_3$ and $k_4$ are very high, but related by $K_{trans} = k_3/k_4$. Hence, only $K_{trans}$ is estimated. The high $k_3$ and $k_4$ values denote the high mobility of O atoms in the lattice of the catalyst. The $K_{trans}$-value higher than 1 corresponds to bulk O atoms being more stable than the surface O atoms, as expected.

## 5.2. Propane feed

### 5.2.1. Single-pulse experiments

*5.2.1.1. Temperature range 723–873 K.* The experimental and calculated propane and $CO_2$ responses for all investigated catalysts are presented in Fig. 5. The parameter estimates for the CuO–$CeO_2$/γ-$Al_2O_3$ catalyst will be discussed first, while the estimates for the two other catalysts will be assessed and compared in Section 6, see Table 5.

The parameter estimates, related to the $CO_2$ product responses in case of propane feed, can be compared to the estimates obtained for a single-pulse experiment with $CO_2$ as feed. The desorption of $CO_2^{*,s}$ from the catalyst surface is temperature dependent for both propane and $CO_2$ feed. However, the activation energy in the former case is much higher, i.e., 127.3 ± 1.4 kJ/mol compared to 57.8 ± 0.7 kJ/mol, leading to a lower desorption rate coefficient, $k_{17}$, if propane is pulsed over the catalyst bed. This results in a

**Table 4**
Estimates for the rate coefficients of $O_2$ adsorption and desorption at 773 K, the activation energies and the ratios of $k_3$ to $k_4$, $K_{trans}$, with their 95% confidence intervals obtained by non-isothermal single-response regression of $O_2$ single-pulse experiments between 623 and 873 K over pre-oxidized catalysts, see Fig. 2a for numbering of reactions.

| | CuO–$CeO_2$/γ-$Al_2O_3$ | CuO/θ-$Al_2O_3$ | $CeO_2$/γ-$Al_2O_3$ |
|---|---|---|---|
| $k_1$ (m$^3$ kg mol$^{-2}$ s$^{-1}$) | 220.9 ± 6.1 | 1074.1 ± 45.5 | 13.7 ± 0.6 |
| $E_{a,1}$ (kJ mol$^{-1}$) | 66.2 ± 1.2 | 92.4 ± 2.5 | 152.8 ± 4.1 |
| $k_2$ (kg mol$^{-1}$ s$^{-1}$) | (10.0 ± 3.9) × 10$^{-3}$ | (2.9 ± 1.0) × 10$^{-1}$ | (1.8 ± 0.9) × 10$^{-3}$ |
| $E_{a,2}$ (kJ mol$^{-1}$) | –[a] | –[a] | –[a] |
| $K_{trans}$ (–) | 76.3 ± 16.6 | 578.5 ± 0.5 | 23.7 ± 0.1 |
| $F$ (10$^4$) | 3.60 | 0.85 | 1.19 |
| $\rho_{max}$ (–) | 0.93 | 0.50 | 0.29 |

[a] Not significantly different from 0 at 95% probability level.

longer tail in the $CO_2$ response if formed as product, compared to the $CO_2$ response tail following a $CO_2$ feed, see Fig. 5a, and causes a larger deficit in the carbon balance, especially at lower temperatures. The possible formation of several kinetically significant intermediates from propane before the formation of $CO_2^{*,s}$ cannot be the cause of the slower $CO_2$ response as the experimental data can be well described by only considering $CO_2^{*,s}$ as kinetically significant intermediate between propane and $CO_2$, see Section 4.2.1. This implies that once propane is activated, the formed intermediates instantaneously transform to $CO_2^{*,s}$ which desorbs slowly. It is possible that the $CO_2^{*,s}$ species are different if these originate indirectly from propane or directly from adsorbed $CO_2$, giving rise to the observed difference in their desorption rate. Alternatively, different active sites can be involved in the activation of propane and the subsequent production of $CO_2^{*,s}$ compared to the active sites involved in the adsorption/desorption of admitted $CO_2$.

The observed difference in the value of the rate coefficient of the $CO_2^{*,s}$ dissociation, $k_{18}$, if propane, see Table 5, or alternatively $CO_2$, i.e., 122.8 ± 2.5 kg mol$^{-1}$ s$^{-1}$, is pulsed can also be attributed to the difference in origin of the $CO_2^{*,s}$ species, or to the involvement of different active sites. Clearly, the more difficult the $CO_2^{*,s}$ species desorb from the catalyst surface and hence the stronger these species are bound, the easier these are dissociated. This dissociation of adsorbed $CO_2$ to $CO^{*,s}$ and $O^{*,s}$, step (18) from Table 3, is found to be temperature independent. Although this step is reversible through step (19), the forward reaction rate coefficient, $k_{18}$, is higher than the reverse, $k_{19}$, implying that the $O^{*,s}$ atoms created upon dissociation of $CO_2$ will have a sufficiently large lifetime to be involved in the propane total oxidation.

*5.2.1.2. Temperature range 623–873 K.* Focusing on the propane responses alone, the propane single-pulse data can be modeled over the whole temperature range by a single-response regression. The agreement between the experimental and the calculated responses can be assessed from Fig. 6. Similar to the regression of the $O_2$ single-pulse experiments, a very broad temperature range can be well described with a single mechanism and a single set of kinetic parameters. The parameter estimates will be evaluated based on

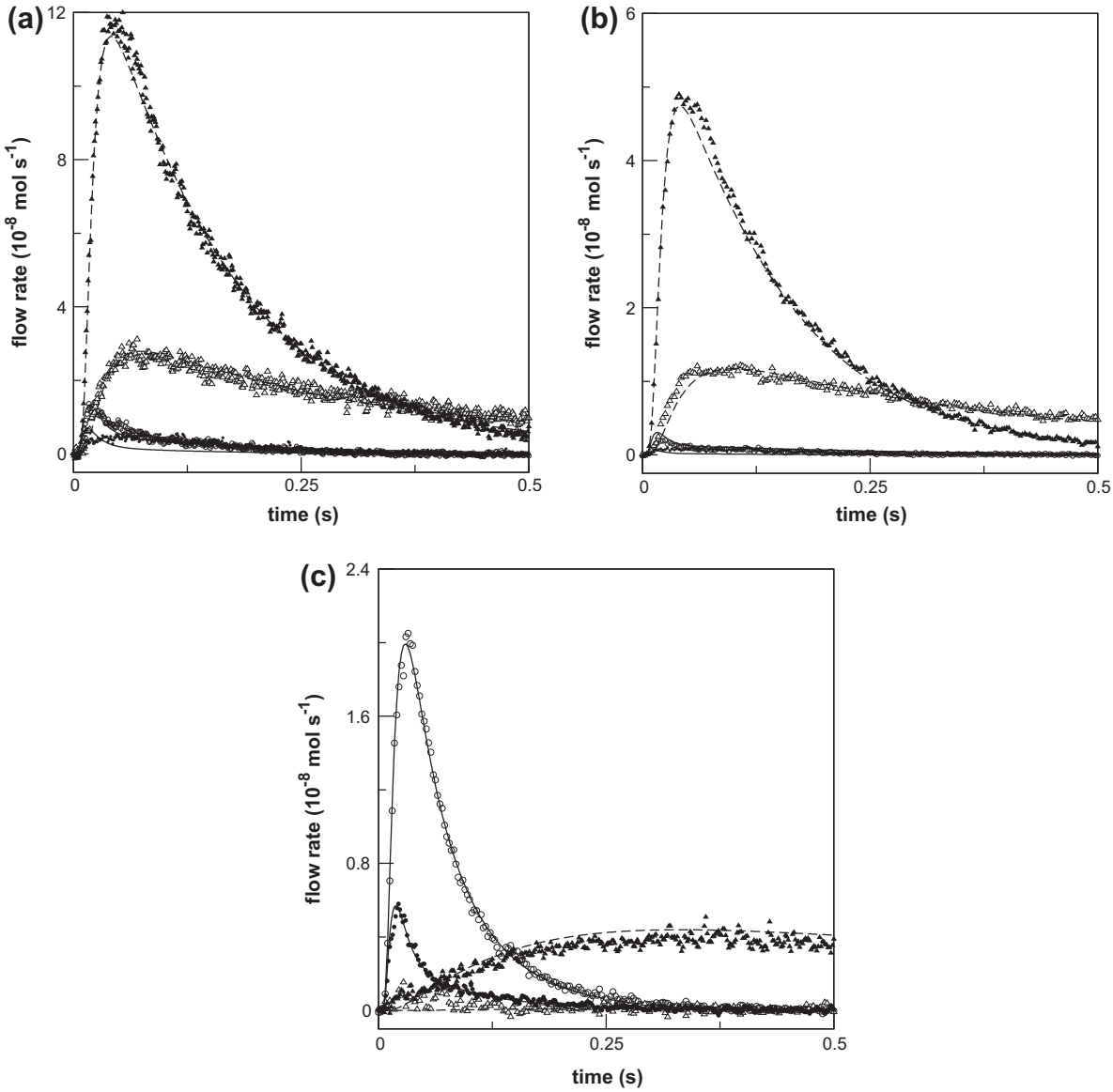


**Fig. 5.** Propane and $CO_2$ reactor exit flow rates corresponding to propane single-pulse experiments over pre-oxidized CuO–$CeO_2$/γ-$Al_2O_3$ (a), CuO/θ-$Al_2O_3$ (b), and $CeO_2$/γ-$Al_2O_3$ (c) at 773 K (empty symbols) and 873 K (full symbols). (●) Experimental $C_3H_8$ responses; (▲) experimental $CO_2$ responses; (–) $C_3H_8$ and (- - -) $CO_2$ responses calculated with parameter estimates listed in Tables 1 and 5, obtained by isothermal single-response regression of $O_2$ responses and non-isothermal multi-response regression of $C_3H_8$ and $CO_2$ responses, and Eqs. (1)–(4) with the corresponding net production rates, Eqs. (22)–(28).

**Table 5**
Estimates of rate coefficients at 773 K and activation energies with their 95% confidence intervals obtained by non-isothermal multi-response regression of propane single-pulse experiments between 723 and 873 K over pre-oxidized catalysts, see Fig. 2b for numbering of reactions.

| | $CuO–CeO_2/\gamma\text{-}Al_2O_3$ | $CuO/\theta\text{-}Al_2O_3$ | $CeO_2/\gamma\text{-}Al_2O_3$ |
|---|---|---|---|
| $k_5$ ($m^3\ mol^{-1}\ s^{-1}$) | 4.8 ± 0.1 | 34.4 ± 0.5 | 0.7 ± 0.1 |
| $E_{a,5}$ (kJ $mol^{-1}$) | 16.5 ± 1.7 | 24.7 ± 1.2 | 158.4 ± 1.9 |
| $k_6$ ($s^{-1}$) | 15.9 ± 0.4 | 18.5 ± 0.2 | 25.9 ± 0.7 |
| $E_{a,6}$ (kJ $mol^{-1}$) | –[a] | –[a] | –[a] |
| $k_7$ ($m^3\ kg\ mol^{-2}\ s^{-1}$) | 22.6 ± 0.5 | 458.3 ± 5.7 | 41.7 ± 0.3 |
| $E_{a,7}$ (kJ $mol^{-1}$) | 64.3 ± 1.9 | 94.7 ± 1.3 | 126.0 ± 0.7 |
| $k_{17}$ ($s^{-1}$) | 23.9 ± 0.9 | 17. 6 ± 0.2 | $(3.0 \pm 0.1) \times 10^{-2}$ |
| $E_{a,17}$ (kJ $mol^{-1}$) | 127.3 ± 1.4 | 125.3 ± 0. 7 | 169.6 ± 1.5 |
| $k_{18}$ ($kg\ mol^{-1}\ s^{-1}$) | $(1.2 \pm 0.1) \times 10^3$ | $(1.1 \pm 0.1) \times 10^3$ | 3.9 ± 0.1 |
| $E_{a,18}$ (kJ $mol^{-1}$) | –[a] | –[a] | –[a] |
| $k_{19}$ ($kg\ mol^{-1}\ s^{-1}$) | 14.1 ± 0.6 | 72.6 ± 1.1 | –[a] |
| $E_{a,19}$ (kJ $mol^{-1}$) | –[a] | –[a] | –[a] |
| $F$ ($10^4$) | 9.98 | 54.21 | 19.99 |
| $\rho_{max}$ (−) | 0.77 | 0.87 | −0.94 |

[a] Not significantly different from 0 at 95% probability level.

the single-response regression, see Table 6, as the latter covers a broader temperature range.

The associative adsorption of propane, step (5) from Table 3, is found to be reversible, step (6), but not at equilibrium. Indeed, varying the absolute values of $k_5$ and $k_6$ while fixing their ratio resulted in different propane shapes, which did not adequately describe the observed responses. It can be concluded that the propane response is not solely dependent on the value of the equilibrium coefficient, $K$, but also depends on the absolute values of $k_5$ and $k_6$ in accordance with Rothaemel et al. [34].

As these two steps do not lead to formation of $CO_2$, mainly step (7) from Table 3 is important concerning the activity of the catalyst for the total oxidation of propane. This kinetically significant step in the activation of propane on two lattice oxygen atoms leading to $CO_2$ has an activation energy, $E_{a,7}$, of 62 kJ $mol^{-1}$ which is comparable to other values reported in literature for propane oxidation

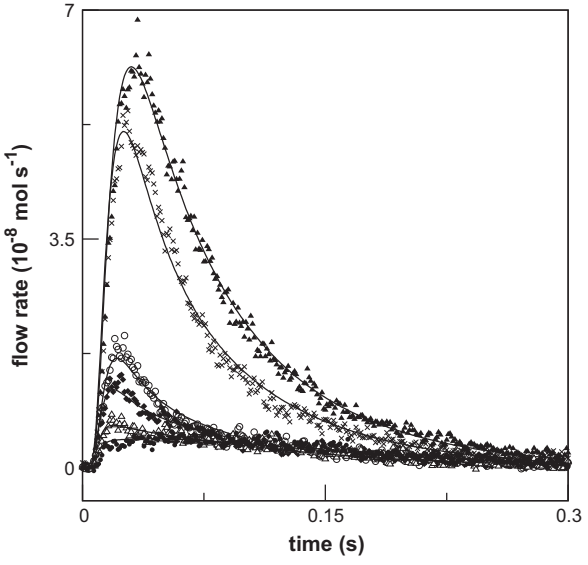


**Fig. 6.** Propane reactor exit flow rates corresponding to propane single-pulse experiments over pre-oxidized $CuO–CeO_2/\gamma\text{-}Al_2O_3$ at (▲) 623, () 673, (○) 723, (♦) 773, (Δ) 823, and (●) 873 K. Experimental $C_3H_8$ responses are presented by symbols; (–) $C_3H_8$ responses calculated with parameter estimates listed in Tables 1 and 6, obtained by isothermal single-response regression of $O_2$ responses and non-isothermal single-response regression of $C_3H_8$ responses, and Eqs. (1)–(4) with the corresponding net production rates, Eqs. (22), (24), and (25). $CO_2$ desorption is neglected.

**Table 6**
Estimates of rate coefficients at 773 K, activation energies and corresponding reaction time scale at 773 K with their 95% confidence intervals obtained by non-isothermal (623–873 K) or isothermal single-response regression of propane single-pulse and multi-pulse experiments over pre-oxidized $CuO–CeO_2/\gamma\text{-}Al_2O_3$, see Fig. 2b for numbering of reactions.

| | Single pulse | Multi pulse |
|---|---|---|
| $k_5$ ($m^3\ mol^{-1}\ s^{-1}$) | 5.9 ± 0.2 | 2.8 ± 0.6 |
| $E_{a,5}$ (kJ $mol^{-1}$) | 90.1 ± 1.4 | –[a] |
| $k_6$ ($s^{-1}$) | 39.9 ± 1.6 | 33.2 ± 8.7 |
| $E_{a,6}$ (kJ $mol^{-1}$) | 6.8 ± 1.8 | –[a] |
| $k_7$ ($m^3\ kg\ mol^{-2}\ s^{-1}$) | 24.5 ± 0.3 | 30.8 ± 7.6 |
| $E_{a,7}$ (kJ $mol^{-1}$) | 62.3 ± 0.4 | –[a] |
| $\tau_7$ (s) | $(3.0 \pm 0.1) \times 10^{-3}$ | $(2.4 \pm 0.6) \times 10^{-3}$ |
| $F$ ($10^4$) | 20.38 | 5.22 |
| $\rho_{max}$ (−) | 0.81 | 0.53 |
| ΔBIC (−)[b] | 19,489 | 0 |

[a] No activation energy is determined as only isothermal regression was performed.
[b] Values relative to the BIC value obtained for the regression of propane multi-pulse experiments.

[35,36]. The rate coefficient of this step, $k_7$, estimated by the single-response regression corresponds very well with the estimate obtained by the multi-response regression. This does not only apply to the temperature reported in Tables 5 and 6, i.e., 773 K, but to the complete common temperature range. As expected, the methylene C–H bond activation, step (7), is somewhat slower than the associative propane adsorption, step (5). This is indicated by the lower rate coefficient, $k_7$, compared to $k_5$, if expressed in $s^{-1}$, leading to a value of $3.3 \times 10^2$ and $8.1 \times 10^2$ $s^{-1}$.

### 5.2.2. Multi-pulse experiments

Describing the propane multi-pulse experiments with the parameters calculated for the propane single-pulse experiments resulted in an overestimate of the propane responses as clearly demonstrated in Fig. 7a. The single-pulse experiments only take into account the consumption of surface oxygen atoms, $O^{*,S}$. If, additionally, transport of oxygen atoms from surface to bulk and vice versa, steps (3) and (4) in Table 2, is taken into account, the observed propane evolution can be described adequately, see Fig. 7b. This indicates that not only surface oxygen atoms are available for oxidation during a multi-pulse experiment, but O atoms originating from the bulk of the catalyst also convert propane. Still, the persistent evolution of the propane responses indicates that this transport cannot fully compensate for the consumption of

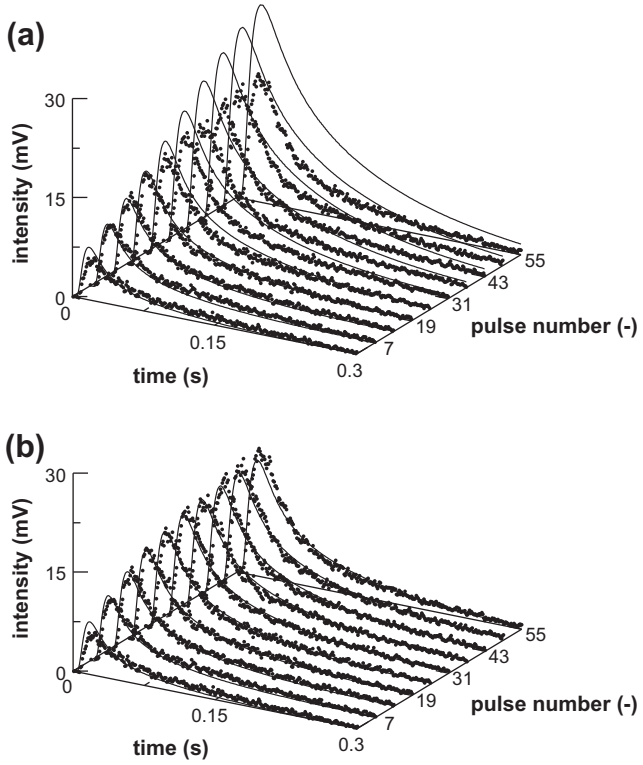


**Fig. 7.** Evolution of propane responses at 773 K over pre-oxidized CuO–$CeO_2$/γ-$Al_2O_3$ corresponding to a $C_3H_8$/Kr multi-pulse experiment consisting of 60 pulses with the $C_3H_8$ response monitored every six pulses. (●) Experimental $C_3H_8$ responses; (–) $C_3H_8$ responses calculated with parameter estimates reported in Tables 1 and 6, for (a) propane single-pulse experiments, applying Eqs. (1)–(4) with corresponding net production rates, Eqs. (22), (24), and (25), and for (b) a propane multi-pulse experiment, applying Eqs. (1)–(4) with the corresponding net production rates, Eqs. (29)–(32).

available surface atoms on the time scale of the conducted multi-pulse experiment. In order to clarify this, the different time scales of the important processes can be calculated, applying following equations:

$$\tau_7 = \frac{\varepsilon_c L_c S}{k_7 (C^0_{O^{*,s}})^2 W_c} \tag{45}$$

for the time scale of activation of propane, and Eq. (46) for the time scale of the transport of O atoms from the bulk to the surface:

$$\tau_4 = \frac{1}{k_4} \tag{46}$$

To calculate the time scale, $\tau_7$, the concentration of $O^{*,S}$ must remain more or less constant. This is clearly not the case during the multi-pulse experiments as previously discussed. Hence, the initial value of $O^{*,S}$, $C^{\circ}_{O^*,s}$, is applied to calculate the time scale implying that the scale is only applicable to the first pulse of the multi-pulse experiment. This restriction is the main reason for the good agreement between the time scale calculated based on the single-pulse experiments on one hand and the multi-pulse experiments on the other hand, see Table 6. It is obvious that the reaction time scale $\tau_7$ listed in Table 6 is several orders of magnitude smaller than the transport time scale, $\tau_4$, which amounts to 565 ± 197 s for the transport of $O^{*,b}$ to $O^{*,S}$ atoms. In the course of a multi-pulse experiment, this transport is fast enough to influence the activity of the catalyst toward propane oxidation, but is too slow to create a stable activity during 60 pulses.

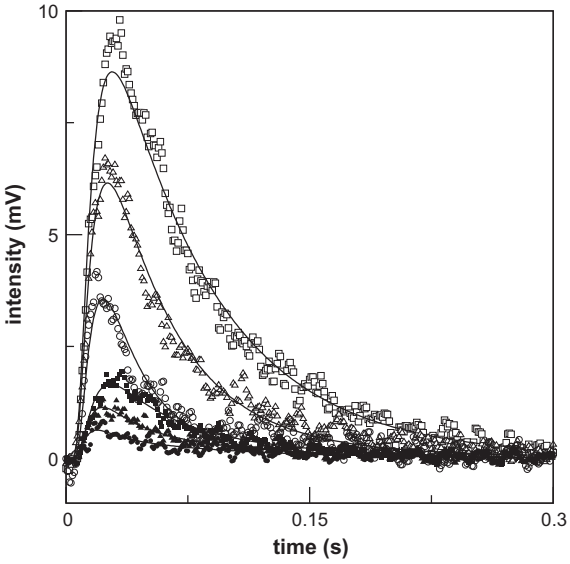


**Fig. 8.** Propane (full symbols) and $O_2$ (empty symbols) responses corresponding to propane/$O_2$ single-pulse experiments over pre-oxidized CuO–$CeO_2$/γ-$Al_2O_3$ at (■) 623, (▲) 673, and (●) 723 K. Experimental responses are presented by symbols; (–) $C_3H_8$ and $O_2$ responses calculated with parameter estimates listed in Tables 1, 4, 6 and 7, and Eqs. (1)–(4) with the corresponding net production rates, Eqs. (38)–(44).

**Table 7**
Estimates of rate coefficients at 723 K and activation energies with their 95% confidence intervals obtained by non-isothermal multi-response regression of propane/$O_2$ single-pulse experiments between 623 and 723 K over pre-oxidized CuO–$CeO_2$/γ-$Al_2O_3$, see Fig. 2c for numbering of reactions. The parameter values $K_{trans} = k_3/k_4$, $k_5$, $k_6$, and $k_7$ are fixed and listed in Tables 4 and 6.

| | |
|---|---|
| $k_{20}$ ($m^3$ kg $mol^{-2}$ $s^{-1}$) | 62.9 ± 51.0 |
| $E_{a,20}$ (kJ $mol^{-1}$) | 69.3 ± 48.8 |
| $k_{1a}$ ($m^3$ kg $mol^{-2}$ $s^{-1}$) | (2.2 ± 0.1) × $10^2$ |
| $E_{a,1a}$ (kJ $mol^{-1}$) | 137.7 ± 1.9 |
| $k_{2a}$ (kg $mol^{-1}$ $s^{-1}$) | (5.2 ± 1.1) × $10^{-4}$ |
| $E_{a,2a}$ (kJ $mol^{-1}$) | –[a] |
| $k_{1b}$ ($m^3$ $kg^{-1}$ $s^{-1}$) | (1.6 ± 0.5) × $10^4$ |
| $E_{a,1b}$ (kJ $mol^{-1}$) | 128.3 ± 6.5 |
| $k_{2b}$ ($s^{-1}$) | (6.5 ± 2.0) × $10^6$ |
| $E_{a,2b}$ (kJ $mol^{-1}$) | –[a] |
| $F$ ($10^4$) | 2.75 |
| $\rho_{max}$ (–) | 0.98 |

[a] Not significantly different from 0 at 95% probability level.

Although the reaction time scale, $\tau_7$, is very small, it is measurable as it lies within the window of measurable rate coefficients or corresponding time scales derived by Huinink et al. [37] for TAP single-pulse experiments:

$$1 \geqslant \tau_{process} \geqslant 10^{-4} s \tag{47}$$

Such a small time scale for reaction illustrates the high activity of this catalyst for propane activation.

### 5.3. Oxygen/propane mixture

In Fig. 8, it is demonstrated that $O_2$ and propane responses corresponding to single-pulse experiments with an $O_2$/propane mixture over pre-oxidized CuO–$CeO_2$/γ-$Al_2O_3$ can be very well described by the combined reaction network for reduction and oxidation presented in Section 4.4. The corresponding parameter estimates are shown in Table 7.

If a propane/$O_2$ mixture is introduced, both weakly bound oxygen, $O_{weak}$, and lattice oxygen atoms, $O^{*,S}$, activate propane. As the

value for $k_{20}$ reported in Table 7 at 723 K is higher than $k_7$ reported in Table 6 at 773 K, it can be concluded that $O_{weak}$ atoms are more active toward total oxidation than the $O^{*,S}$ atoms. Despite this higher activity, the propane activation rate on the $O_{weak}$ atoms is lower compared to the rate on the $O^{*,S}$ atoms, because of the much lower concentration of the former atoms. This is in line with the high estimated desorption rate coefficient of the $O_{weak}$ atoms, $k_{2b}$ in Table 7, limiting their influence, especially on a larger time scale. The regeneration of the $O^{*,S}$ atoms, presented by $k_{1a}$ in Table 7, is slower than the creation of the $O_{weak}$ atoms through $k_{1b}$, which is partially compensated by the faster desorption of the latter. It must be mentioned that before comparing these rate coefficients, both values were expressed in $s^{-1}$. Again, no temperature dependent desorption processes could be estimated for the same reason as explained in Section 5.1.2. The presence of $O_{weak}$ atoms increases only slightly the concentration of catalytically active sites under total oxidation conditions, so the higher observed activity is the result of their higher reactivity.

## 6. Single metal oxides

The mechanism of total oxidation on single metal oxides is thought to be similar to that on the mixed metal oxide [2]. Application of the reaction networks of oxidation, see Section 4.1, and reduction, see Section 4.2, derived for the CuO–$CeO_2$/γ-$Al_2O_3$ catalyst to the experimental responses over the single oxide catalysts allowed a similarly good description of the experimental data, see Fig. 5b and c for the propane and $CO_2$ responses over CuO/θ-$Al_2O_3$ and $CeO_2$/γ-$Al_2O_3$, respectively.

For the CuO/θ-$Al_2O_3$ catalyst, significant parameter estimates were found for all the steps considered significant on CuO–$CeO_2$/γ-$Al_2O_3$. For the $CeO_2$/γ-$Al_2O_3$ catalyst, only the recombination of $CO^{*,S}$ and $O^{*,S}$, reaction (19), was not found to be significant, see Table 5.

### 6.1. Oxygen feed

The average values for the initial concentration of reduced active sites, $C^{\circ}_{*,S}$, for the single metal oxides, listed in Table 1 can be compared to the value obtained for CuO–$CeO_2$/γ-$Al_2O_3$. Clearly, the $CeO_2$/γ-$Al_2O_3$ catalyst releases its surface oxygen atoms more easily compared to the other catalysts as the ratio of the initially reduced active sites to the total number of surface lattice oxygen atoms is the highest, i.e., from 58% to 63%, depending on the considered temperature range. For the CuO/θ-$Al_2O_3$ catalyst, the ratio varies from 34% to 48%, which is lower than for $CeO_2$/γ-$Al_2O_3$, but higher than for the mixed metal oxide.

The activation of $O_2$ by adsorption on two reduced catalytic sites is an activated process for all catalysts, see Table 4. The lowest value of $E_{a,1}$ was obtained for CuO–$CeO_2$/γ-$Al_2O_3$, i.e., 66.2 kJ $mol^{-1}$ compared to 92.4 kJ $mol^{-1}$ for the CuO/θ-$Al_2O_3$ and 152.8 kJ $mol^{-1}$ for the $CeO_2$/γ-$Al_2O_3$. The latter high activation energy resulted in a much lower $k_1$-value for the $O_2$ activation on $CeO_2$/γ-$Al_2O_3$. Just as for CuO–$CeO_2$/γ-$Al_2O_3$, the rate coefficient of the desorption of $O^{*,S}$ on the single metal oxides is low compared to the value of adsorption. The corresponding activation energy of desorption cannot be estimated significantly different from zero at 95% probability level.

For both Cu- and Ce-based single metal oxide catalysts, a high O mobility is demonstrated by the estimated exchange between the surface and bulk O atoms through a significant $K_{trans}$-value, see Table 4. For the supported $CeO_2$, a lower $K_{trans}$-value was estimated compared to the supported CuO. This implies that the relative stability of the surface lattice O atoms compared to the bulk O atoms is higher over the $CeO_2$ catalyst, improving the availability of the active O atoms. Given the combination of high O mobility with higher availability, one would expect that $CeO_2$/γ-$Al_2O_3$ is a better performing catalyst for total oxidation than CuO/θ-$Al_2O_3$. However, a good catalyst should also be efficient in activating the hydrocarbon to be oxidized, in casu propane.

### 6.2. Propane feed

For the ceria catalyst, a much higher activation energy is found for the rate coefficient corresponding to propane activation presented by $E_{a,7}$ in Table 5, resulting in a much lower $k_7$-value. Combined with the much lower estimate for the $O_2$ activation, presented by $k_1$ in Table 4, it is found that the activation of both reactants involved in the total oxidation is more difficult over $CeO_2$/γ-$Al_2O_3$. Hence, it can be concluded that the $CeO_2$ catalyst has a much lower activity compared to the CuO catalyst. Ceria is known to have a low activity, either pure or supported [39]. In contrast, copper oxide catalysts are typically good catalysts for VOC destruction [5] which is confirmed in this study.

The non-significant $k_{19}$-value for $CeO_2$/γ-$Al_2O_3$ can be understood if the role of ceria as activator of $CO_2$ is considered [9], together with the very high mobility of oxygen atoms within the ceria lattice. If $CO_2^{*,S}$ is dissociated to $CO^{*,S}$ and $O^{*,S}$ on ceria via elementary step (18), the O atoms will be transported along the surface where they can participate in the total oxidation reaction, rather than recombine to form $CO_2^{*,S}$ through elementary step (19). Hence, no significant estimate for the recombination of $CO^{*,S}$ and $O^{*,S}$, $k_{19}$, could be determined. This is in line with Sharma et al. [38] who stated that $CO_2$ is adsorbed on $Ce^{3+}$ sites and is able to oxidize the reduced ceria. The high $CO_2$ dissociation activity of

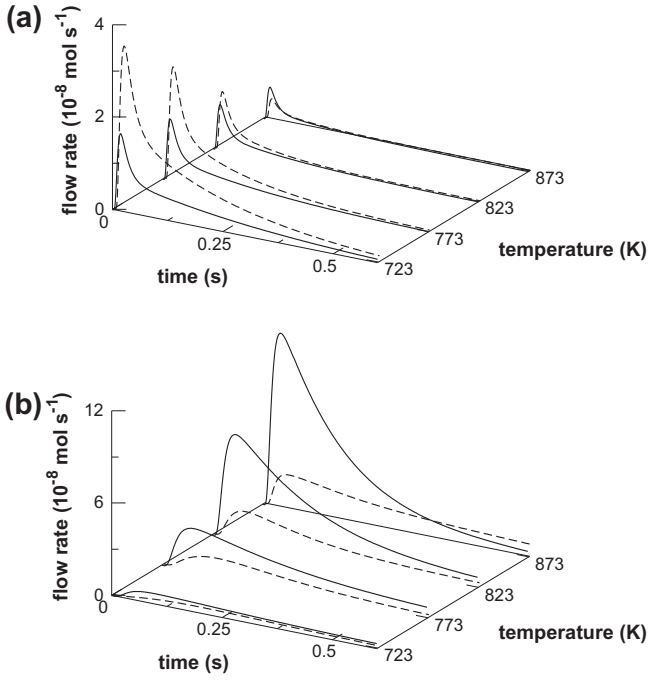


**Fig. 9.** Propane (a) and $CO_2$ (b) reactor exit flow rates corresponding to propane single-pulse experiments between 723 and 873 K over pre-oxidized catalyst. (–) $C_3H_8$ and $CO_2$ responses over pre-oxidized CuO–$CeO_2$/γ-$Al_2O_3$ calculated with parameter estimates for CuO–$CeO_2$/γ-$Al_2O_3$ listed in Tables 1 and 5; (- - -) $C_3H_8$ and $CO_2$ responses over pre-oxidized (CuO + $CeO_2$)/γ-$Al_2O_3$, a virtual catalyst consisting of the two metal oxides supported on $Al_2O_3$ without interaction between the oxides. The latter responses are calculated with a combination of the parameter estimates for CuO/θ-$Al_2O_3$ and $CeO_2$/γ-$Al_2O_3$ listed in Tables 1 and 5. All responses are calculated by applying the reactor model given by Eqs. (1)–(4) with the corresponding net production rates, Eqs. (22)–(28).

the $CeO_2/\gamma$-$Al_2O_3$ catalyst, implying a high interaction with the latter, corresponds well with the low-estimated value of the $CO_2^{*,S}$ desorption coefficient, $k_{17}$ in Table 5.

## 7. Comparison of CuO–$CeO_2/\gamma$-$Al_2O_3$ with a physical binary mixture of single metal oxides

In order to assess the synergy of CuO and $CeO_2$ in CuO–$CeO_2/\gamma$-$Al_2O_3$, its performance is compared with a virtual mixed metal oxide catalyst under reduction conditions, denoted as (CuO + $CeO_2$)/$\gamma$-$Al_2O_3$, containing identical amounts of $O^{*,S}$ atoms as on CuO–$CeO_2/\gamma$-$Al_2O_3$, either related to CuO or to $CeO_2$, see Table 1. The initial concentration of reduced surface sites, $C^{\circ}_{*,S}$, is calculated assuming that an identical percentage of the total surface O atoms as on the single metal oxides will desorb from CuO and $CeO_2$ before starting the propane single-pulse experiments, i.e., 34–48% and 58–63%. In this simulation, the kinetic parameters corresponding to the single metal oxides are inserted into the kinetic model for the virtual catalyst, a priori assuming that no interaction between $CeO_2$ and CuO will influence the activity.

Fig. 9 shows the calculated propane and $CO_2$ responses corresponding to the simulation of the virtual (CuO + $CeO_2$)/$\gamma$-$Al_2O_3$ catalyst and the investigated CuO–$CeO_2/\gamma$-$Al_2O_3$. The higher propane responses over the virtual catalyst compared to the responses over CuO–$CeO_2/\gamma$-$Al_2O_3$, correspond to a conversion which is lower over a catalyst without interaction between the two metal oxides. The opposite applies for the $CO_2$ responses, which are obviously much higher for the actual catalyst, demonstrating its higher activity. Clearly, combining ceria with copper oxide on alumina increases the catalytic activity.

Based on the experiments over $CeO_2/\gamma$-$Al_2O_3$, it is found that ceria plays an important role in the O supply for the reaction, originating either from $O_2$ or $CO_2$ [11]. However, this is not the only function of ceria in the CuO–$CeO_2/\gamma$-$Al_2O_3$ catalyst. Indeed, focusing on the propane and $CO_2$ responses at 873 K in Fig. 9, it is observed that the propane conversions are more or less equal, while the $CO_2$ responses over CuO–$CeO_2/\gamma$-$Al_2O_3$ are higher at that temperature, indicating a higher $CO_2$ desorption rate. The increased desorption rate implies a weaker interaction and thus as previously stated, a lower dissociation activity toward $CO^{*,S}$ and $O^{*,S}$. This in turn implies that combining $CeO_2$ with CuO diminishes the production of O atoms from $CO_2$. Hence, increased O supply from dissociating $CO_2$ is not the motivation for adding ceria to the catalyst. Besides, over $CeO_2/\gamma$-$Al_2O_3$, activation of propane is observed, indicating that the role of ceria is not limited to that of O supplier. Likewise, propane activation is also confirmed over the CuO/$\theta$-$Al_2O_3$, with a higher rate than over the $CeO_2/\gamma$-$Al_2O_3$ catalyst. Next to that function of propane activation, a high O mobility was established, indicating that CuO has other functions than merely activating the hydrocarbon. It is thus believed that the redox activity for CuO–$CeO_2/\gamma$-$Al_2O_3$ is determined by reduction and oxidation properties of both copper oxide and ceria separately, as well as combined, and therefore influenced by the strong interaction between these phases [40]. As the activation energy for the propane C–H bond activation, $E_{a,7}$ in Table 5, for the mixed metal oxide is lower than the activation energies on the single metal oxides, it is clear that the interactive combination of CuO and $CeO_2$ results into reactive O atoms. This is also indicated by the different activation energies for the dissociative $O_2$ adsorption over all catalysts. The enhancement of the catalytic activity is thus a result of an interaction between the two oxide phases and is associated with a change in the reactivity of the involved O atoms. This is in contrast to Radwan et al. [41] who state that doping of CuO/$Al_2O_3$ solids with ceria enhanced the catalytic activity solely by an increase in the concentration of active sites with identical energetic properties.

## 8. Conclusions

Applying a transient technique provides experimental data for description of reaction networks and determination of kinetic models that can adequately describe the redox processes, both combined and individually, occurring on metal oxides. Limiting the reaction networks to the reduction and oxidation on the surface layer of the catalysts allows to describe adequately the experimental data. Besides the kinetic parameters, the initial concentration of reduced active sites can also be estimated by regression of $O_2$ responses corresponding to an $O_2$/Ar single-pulse experiment over a pre-oxidized catalyst. The surface oxygen atoms are not the only active atoms available, as an extra amount of O atoms originates from the catalyst bulk. An exchange between these atoms can also be modeled during propane as well as oxygen-pulse experiments. In the former case, the transport from the bulk to the surface is significantly slower than the rate of consumption of surface O atoms, leading to a significant evolution in the propane responses during multi-pulse experiments.

If instead of pure propane or $O_2$, a propane/$O_2$ mixture is introduced, the performance of the catalyst improves due to weakly bound oxygen atoms, created over pre-oxidized catalyst. Introduction of $CO_2$ over a reduced CuO–$CeO_2/\gamma$-$Al_2O_3$ catalyst leads to re-oxidation through dissociation to $CO^{*,S}$ and $O^{*,S}$ species. This $CO_2$ dissociation also occurs if $CO_2$ is formed as product during propane oxidation. However, this does not significantly contribute to the propane oxidation on a time scale of a single-pulse experiment, because of the limited amount of $O^{*,S}$ atoms produced from $CO_2$ as product, compared to the much higher initial amount of $O^{*,S}$ atoms in the catalyst.

The supported CuO catalyst shows a high rate of first C–H bond activation in propane during the reduction of the catalyst, and a high ability to restore its initial activity by $O_2$ activation and subsequent re-oxidation of the catalyst. The ceria-based catalyst is less active for both mentioned processes. However, the highest activity is established for the mixed metal oxide catalyst, i.e., the CuO–$CeO_2/\gamma$-$Al_2O_3$. The addition of ceria to the copper oxide catalyst results in a close interaction between these two oxide phases, leading to an increased catalytic activity.

## Acknowledgment

This work was performed in the framework of a Concerted Research Action (GOA) of Ghent University and was supported by the Long Term Structural Methusalem Funding by the Flemish Government.

## References

[1] S.H. Taylor, C.S. Heneghan, G.J. Hutchings, I.D. Hudson, Catal. Today 59 (2000) 249.
[2] J.J. Spivey, Ind. Chem. Res. 26 (1987) 2165.
[3] R.K. Grasselli, Top. Catal. 21 (2002) 79.
[4] G.J. Hutchings, S.H. Taylor, Catal. Today 49 (1999) 105.
[5] E.M. Cordi, P.J. O'Neill, J.L. Falconer, Appl. Catal. B 14 (1997) 23.
[6] W. Liu, M. Flytzani-Stephanopoulos, J. Catal. 153 (1995) 304.
[7] A. Trovarelli, C. de Leitenburg, M. Boaro, G. Dolcetti, Catal. Today 50 (1999) 353.
[8] A. Trovarelli, Catal. Rev. 38 (1996) 439.
[9] O. Demoulin, M. Navez, J.-L. Mugabo, P. Ruiz, Appl. Catal. B 70 (2007) 284.
[10] J. Chen, Y. Zhan, J. Zhu, C. Chen, X. Lin, Q. Zheng, Appl. Catal. A 377 (2010) 121.
[11] W. Liu, M. Flytzani-Stephanopoulos, J. Catal. 153 (1995) 317.
[12] D. Delimaris, T. Ioannides, Appl. Catal. B 89 (2009) 295.
[13] P.M. Heynderickx, J.W. Thybaut, H. Poelman, D. Poelman, G.B. Marin, J. Catal. 272 (2010) 109.
[14] V. Balcaen, R. Roelant, H. Poelman, D. Poelman, G.B. Marin, Catal. Today 157 (2010) 49.
[15] P.M. Heynderickx, J.W. Thybaut, H. Poelman, D. Poelman, G.B. Marin, Appl. Catal. B 95 (2010) 26.

[16] G. Silversmit, H. Poelman, V. Balcaen, P.M. Heynderickx, M. Olea, S. Nikitenko, W. Bras, P.F. Smet, D. Poelman, R. De Gryse, M.-F. Reyniers, G.B. Marin, J. Phys. Chem. Solids 70 (2009) 1274.
[17] J.T. Gleaves, J.R. Ebner, T.C. Kuechler, Catal. Rev. Sci. Eng. 30 (1988) 49.
[18] J. Perez-Ramirez, E.V. Kondratenko, Catal. Today 121 (2007) 160.
[19] J.T. Gleaves, G. Yablonsky, X. Zheng, R. Fushimi, P.L. Mills, J. Mol. Catal. A: Chem. 315 (2010) 108.
[20] S.O. Shekhtman, G.S. Yablonsky, S. Chen, J.T. Gleaves, Chem. Eng. Sci. 54 (1999) 4371.
[21] V. Balcaen, I. Sack, M. Olea, G.B. Marin, Appl. Catal. A 371 (2009) 31.
[22] D.W. Marquardt, J. Soc. Ind. Appl. Math. 11 (1963) 431.
[23] G.F. Froment, L.H. Hosten, in: J.R. Anderson, M. Boudart (Eds.), Catalysis Science and Technology, Springer-Verlag, Berlin, 1981.
[24] B.G.M. Vandeginste, D.L. Massart, L.M.C. Buydens, S. De Jong, P.J. Lewi, J. Smeyers-Verbeke, Handbook of Chemometrics and Qualimetrics, Part B, Elsevier, Amsterdam, 2003. p. 323.
[25] G. Schwarz, Ann. Stat. 6 (1978) 461.
[26] O. Dewaele, D. Wang, G.F. Froment, J. Mol. Catal. A: Chem. 149 (1999) 263.
[27] P.L. Mills, H.T. Randall, J.S. McCracken, Chem. Eng. Sci. 54 (1999) 3709.
[28] R.H. Nibbelke, J. Scheerova, M.H.J.M. de Croon, G.B. Marin, J. Catal. 156 (1995) 106.
[29] E. Finocchio, G. Busca, V. Lorenzelli, R.J. Willey, J. Catal. 151 (1995) 204.
[30] A. Pantazidis, S.A. Bucholz, H.W. Zanthoff, Y. Schuurman, C. Mirodatos, Catal. Today 40 (1998) 207.
[31] H.W. Zanthoff, S.A. Bucholz, A. Pantazidis, C. Mirodatos, Chem. Eng. Sci. 54 (1999) 4397.
[32] X. Tang, B. Zhang, Y. Li, Y. Xu, Q. Xin, W. Shen, Appl. Catal. A 288 (2005) 116.
[33] A. Martinez-Arias, M. Fernandez-Garcia, O. Galvez, J.M. Coronado, J.A. Anderson, J.C. Conesa, J. Soria, G. Munuera, J. Catal. 195 (2000) 207.
[34] M. Rothaemel, M. Baerns, Ind. Eng. Chem. Res. 35 (1996) 1556.
[35] V.R. Choudhary, S. Banerjee, S.G. Pataskar, Appl. Catal. A 253 (2003) 65.
[36] M. Baldi, E. Finocchio, F. Milella, G. Busca, Appl. Catal. B 16 (1998) 43.
[37] J.P. Huinink, J.H.B.J. Hoebink, G.B. Marin, Can. J. Chem. Eng. 74 (1996) 580.
[38] G. Aguila, F. Gracia, P. Araya, Appl. Catal. A 343 (2008) 16.
[39] S. Sharma, S. Hilaire, J.M. Vohs, R.J. Gorte, H.-W. Jen, J. Catal. 190 (2000) 199.
[40] A. Martinez-Arias, M. Fernandez-Garcia, J. Soria, J.C. Conesa, J. Catal. 182 (1999) 367.
[41] N.R.E. Radwan, G.A. Fagal, G.A. El-Shobaky, Colloid Surf. A 178 (2001) 277.